2011

CHARACTERIZATION OF HOLLOW PARTICULATE AND GRADED COMPOSITES USING ULTRASONIC TECHNIQUE

Bhaskar Ale
University of Rhode Island, bhaskarale@gmail.com

CHARACTERIZATION OF HOLLOW PARTICULATE AND GRADED COMPOSITES USING ULTRASONIC TECHNIQUE

BY

BHASKAR ALE

A THESIS SUBMITTED IN PARTIAL FULFILLMENT OF THE REQUIREMENTS FOR THE DEGREE OF

MASTER OF SCIENCE

IN

MECHANICAL ENGINEERING AND APPLIED MECHANICS

UNIVERSITY OF RHODE ISLAND

2011

MASTER OF SCIENCE THESIS

OF

BHASKAR ALE

APPROVED:

Thesis Committee:

Major Professor Carl-Ernst Rousseau

K. Wayne Lee

David G. Taggart

Nasser H. Zawia
DEAN OF THE GRADUATE SCHOOL

UNIVERSITY OF RHODE ISLAND
2011

ABSTRACT

An experimental study has been conducted to characterize hollow particulate composites (syntactic foams) using ultrasonic pulse echo techniques. Materials tested for this study consisted of low viscosity epoxy matrix with embeded soda-lime-borosilicate glass micro-balloons of different volume fractions. Three sizes of microballoons ranging from 30-65 microns were tested. Measurements of longitudinal and shear wave speed and attenuation of ultrasonic wave in syntactic foams were taken. These wave speed values were further utilized to calculate the various moduli of the material. After understanding the behavior of syntactic foams for low volume fractions, functionally graded materials (FGM) with linear variation of increasing volume fraction were manufactured and studied. Further quasi-static compression and low velocity impacts were also performed to better understand the static and absorption behavior of both syntactic foams and FGM materials.

It was found that larger microballoon size had higher attenuation values but not necessarily higher wave speeds in syntactic foams. Matrix absorption was the main attenuation parameter. Ultrasonic tests on FGMs suggest higher degree of interaction due to the impedance mismatch between each layer. Lower volume fractions had higher compressive strength than higher volume fractions. This knowledge is important in understanding the bond strength between the particulates and the epoxy matrix. The peak stress in impact loading decreased with increasing volume fraction and was highest for the smallest size microballoon. Peak load of smallest microballoon size FGM was higher than plain syntactic foam of similar density.

ACKNOWLEDGMENTS

I would like to thank my advisor Dr. Carl-Ernst Rousseau for his constant support and guidance during the course of my work. I would also like to thank Department of Homeland Security for providing the funding for my research. I am also thankful to Mr. Tom Nelligan of Olympus NDT for his technical expertise and guidance. I would also like to thank Dr. Shukla for making laboratory equipment available for my research. I would also like to thank the Faculty and Staff in the Department of Mechanical, Industrial and Systems Engineering for their help and encouragement throughout my study. I would also like to thank my lab mate Gifford Plume for his technical advice and discussions. I am also deeply thankful to Rakshya Shrestha for always being there for me throughout my study.

Finally, I am grateful to my parents, sister and close friends for their invaluable support throughout my time at URI.

TABLE OF CONTENTS

LIST OF TABLES

TABLE **PAGE**

LIST OF FIGURES

FIGURE **PAGE**

CHAPTER 1

INTRODUCTION

Advancement in the composite industry is happening day to day. Newer materials with higher strength to weight ratio are increasing in demand by the Army and the Navy. Tanks travelling in water, light aircrafts, core materials for sandwich composites are all looking for lighter, stronger materials. Hollow particulate composites provide that quality.

Whenever there is an impact, stress waves are generated which propagate through the specimen which cause more destruction to the material. Introduction of microballoons or hollow particulates help reduce the affect of stress wave impact by attenuating the wave by scattering and absorption. It is this phenomenon which needs to be more properly understood to better understand attenuating properties of these hollow particulate composites.

This study will characterize hollow particulate composites and graded materials using ultrasonic techniques. The study focuses on the influence of volume fraction and micro-balloon size on the ultrasonic properties of these materials. Attenuation and speed of propagation of ultrasonic waves vary with change in material composition and property and are used for purposes of characterization of materials. Quasi-static compressive tests and low velocity drop tower tests were also carried out and the results compared for full comprehensive understanding of the overall material behavior.

Measurement of wave speed within the material and attenuation of ultrasonic waves are parameters important to its characterization [1]. Attenuation refers to the energy loss associated with the decrease in the stress wave amplitude due to both scattering and absorption [2]. They include scattering at the hollow glass particulates, interface absorption within the epoxy matrix and reflections of wave from surrounding particulates and its interactions, and other losses. Hence, due to the nature of the dispersive medium a proper understanding of the attenuation and wave speed behavior must be properly achieved.

Non destructive testing (NDT) methods are used extensively to evaluate material properties. They are being used in characterization of core materials used in sandwich composites, aerospace and naval industry. Ultrasonic characterization is a novel technique being used in many structural and civil applications for measurement of structural stability and reliability.

Newer synthetic composites are being evaluated with ultrasonics for faster and more reliable characterization. In this study, the focus will be hollow particulate composite materials which have high strength to weight ratio, corrosion resistance, high bending stiffness, and excellent thermal capabilities due to the high strength of the glass microballoons. Epoxy matrix embedded with these hollow glass microballoons have been coined syntactic foams. Syntactic foams also have a broad range of multi-functionality due to their vibration damping characteristics and can also be fabricated into functionally graded materials. Their main advantage is that they can be designed and fabricated according to the physical and mechanical requirements of the desired application.

Numerous quasi-static tests have been carried out to determine static stiffness and yield strength of these materials [3-5]. Recent studies have also shown that wave analysis techniques can be used to determine these dynamic properties [1, 6-8].

Nomenclatures for all specimens in this study are given below. An example of the syntactic foam naming is 'K37-40', where K37 identifies the microballoon type and 40 is the volume percentage of microballoon in syntactic foam. For functionally graded materials 'K37-040-5FGM', where K37 is the microballoon type followed by '040' which denotes 40% as the highest volume percentage of the layers and 5FGM stands for five layered functionally graded material. For 'S60/10000' type microballoon 'S60' is used as the nomenclature in this study.

1.1 Review of Literature

Ultrasonic wave measurements were introduced in mid 1950s. Hirone and Kamigaki [9] calculated the attenuation coefficient of aluminum using ultrasonic waves at a frequency of 2 to 25 MHz. Attenuation coefficients showed a strong dependence on the grain size of the material and frequency.

Further theoretical work was also being conducted evaluating the scattering of plane longitudinal wave by spherical obstacles by Ying and Truell [10]. They discussed three types of obstacles: an isotropically elastic sphere, a spherical cavity, and a rigid sphere for Rayleigh scattering.

Datta [11] further studied the scattering of plane longitudinal waves by a distribution of elastic ellipsoidal inclusions. Using a self consistent approximation and assuming distribution of scatterer centers as a random homogenous function of

position, approximate wave speeds are derived for certain orientations. Various theories and application of wave propagation and scattering are discussed by A. Ishimaru [12].

Wave propagation on random particulate composites was studied by Beltzer, Bert and Striz [13]. They proposed a new method for analysis of wave propagation in random particulate viscoelastic composites. The method computed wave speed based on losses by scattering and viscoelastic losses and using the Kramer-Kronig relationship. Further uses of this relationship are examined in several papers [14-18].

Gubernatis and Domany [19] studied the effects of microstructure on the speed and attenuation of elastic waves in porous media. They developed a set of equations from which effective wave number, wave speed and attenuation can be calculated by knowledge of statistical data. The effective wave number was calculated for some distribution of pore radii.

Ultrasonic attenuation of fiber-reinforced plastics has been studied extensively [20, 22-28]. Martin [20] obtained a qualitative behavior of ultrasonic velocity and attenuation as a function of void and fiber content. Here, void radius is used as the fitting parameter to match calculated results with the experimental values. Further results by Mouritz [21] contradicted Martins Model as the attenuation coefficient measured was less sensitive due to imperfect Rayleigh scattering i.e. waves scattered by a void when they interact with waves scattered by neighboring voids.

The Hale and Ashton's [22] disc void model was capable of predicting high levels of ultrasonic attenuation observed experimentally in voided fiber reinforced plastics. Also they found that the attenuation of unidirectional laminates was greater

than that of fabric laminates. Jeong [23] determined that the strength of laminate systems decreased and attenuation slope increased with increased presence of voids and void geometry. Many have analyzed the wave attenuation in unidirectional viscoelastic composites by a differential scheme [24-27]. The method takes into account both the viscoelastic absorption loss and the wave scattering loss. They identify matrix absorption as the major cause of attenuation. The authors in [24] have also analyzed attenuation of particle reinforced plastics and found that the attenuation decreases monotonically with particle volume fraction when particle radius is small compared to incident wavelength.

Studies related to porosity measurement using ultrasonic techniques have been done by [28, 29]. Nair, Hsu, and Rose [28] estimated the volume fraction by correlating it with the slope of ultrasonic attenuation as a function of frequency. The limits of validity were tested by simulation and comparison with experimental data. Daniel, Wooh and Komsky [29] determined that the measured values of attenuation for the same amount of porosity can vary from specimen to specimen depending upon shape, size, orientation, fabrication, and distribution of porosity.

Recent studies related to ultrasonic velocity and attenuation in solids under different thermal conditions were performed by V. Rajendran, N. Palanivelu and B.K. Chaudhuri [30]. They utilized the pulse through an ultrasonic transmission method. A heater was used to control the heat inside the chamber whereas the transducers were kept outside. The validity of the setup was tested for vanadate bismuth tellurite and vanadate lead semiconducting oxide glasses within a temperature range of 300- 580 K.

Very recently, models have been proposed to define the interaction of ultrasound with particulate composites. Measurement of ultrasonic velocities and attenuation and its relation to frequency for random particulate composites was studied by [31]. Experimental results were compared with the Waterman and Truell Method and the Dynamic generalized self consistent model. It was seen that for low volume fractions both models matched the experimental data but at higher volume fractions a clear correlation could not be obtained. Another recent model by Mylavarapu and Woldesenbet [7] takes into account the effect of particle size, porosity and radius ratio while measuring the ultrasonic attenuation of syntactic foams at low volume fractions. Attenuation losses by absorption, scattering and resonance are integrated into the model. For a frequency of 1 MHz and volume fractions up to 30% good correlation between the experimental and theoretical results were obtained.

Mylavarapu and Woldesenbet [1] also studied the effects of volume fraction of solid sphere in epoxy matrix and the ultrasonic wave attenuation, wave speeds and dynamic Young's modulus were calculated. In the case of solid spheres, particulate composites showed higher attenuation than syntactic foams of similar sphere size due to internal resonance of solid glass spheres. They also showed that the wave speeds of solid particulate composites were also higher than the syntactic foams. Ultrasonic properties of polyester/fly ash composites were also studied by Rohatgi, Matsunaga, and Gupta [32]. Ultrasonic measurements were used to calculate various material properties such as shear modulus, Young's modulus and bulk modulus. Attention was given to decrease in attenuation with increasing volume fractions of fly ash

microballoons. It was seen that the velocity of ultrasound was faster in fly ash microballoons than in the polyester matrix.

Characterization of materials is incomplete without material stress strain behaviors. There have been many studies related to the compressive behaviors of syntactic foams and solid particulate composites [33-39]. Gupta, Woldesenbet and Jerro [33] studied the effects of microballoon radius ratio on the compressive properties of syntactic foams. They noticed that the compressive strength and modulus of syntactic foams increase with a decrease in the microballoon radius. Gupta, Woldesenbet, and Mensah [34] also conducted compressive tests on syntactic foams of different radius ratios and found similar results. They found that orientation during compression affected the peak stress obtained. Tensile properties of vinyl ester microballoon syntactic foams were tested by Gupta, Ye and Porfiri [35]. It was found that the tensile modulus was 15-30% higher than the compressive modulus for same type of syntactic foams. This was due to particle-matrix interfacial debonding and the possibility of particle fracture under compressive loading conditions. Further tests on layered syntactic foams were conducted by Gupta and Ricci [36]. They introduced functionally graded syntactic foams not based on volume fraction but on microballoon wall thickness variation along the length. The new type of FGM showed better control of strength and higher energy absorption values than the volume fraction FGMs.

Bardella and Genna [37] studied the elastic behavior of syntactic foams experimentally, numerically and analytically. They found that the presence of unwanted voids has a significant effect on the elastic moduli of composite. The techniques used for predicting real elastic moduli showed good correlation with

experimental and numerical results. Processing, compression response, and modeling of interpenetrating phase composite (IPC) was done by Jhaver and Tippur [38]. The composite was manufactured by infiltrating uncured syntactic foam into preformed open cell aluminum. Increased values in moduli, yield strength and plateau stress was observed for the IPC syntactic foams. 50% higher energy absorption of silane treated IPC was also observed. The numerical model based on Kelvin cell based 3-D elasto-plastic finite element model was also successful in capturing overall IPC syntactic foam behavior.

Syntactic foam behaviors were studied at higher strain rates of $1s^{-1}$ to $1000s^{-1}$ [40-45]. Hsiao and Daniel [40] studied the strain rate on the compressive and shear behavior of carbon epoxy composite materials. They showed that for cross ply laminates the dynamic stress strain curve stiffened with increasing strain rate. The shear stress-strain behavior also showed that the plateau region of stress increased with increasing strain rate. Low velocity impacts on nanoparticulate syntactic foams were also performed by Woldesenbet [41]. Here nanoclay is mixed with low density syntactic foams and it was observed that at 1% nanoclay volume fraction peak load and highest initiation energy was obtained. Also microcracks were being contained by the stiffer nanoclay particulates in forming major cracks. Li and Jones [42] did similar low velocity impacts on rubberized syntactic foams. The results showed that rubberized syntactic foams were able to absorb higher amount of energy with very little loss in strength. SEM pictures showed that several mechanisms were activated to collaboratively absorb impact energy, including microballoon crushing, interfacial debonding, matrix microcracking, and fiber pull-out; the rubber layer and the

microfibers prevented the microcracks from propagating into macroscopic damage by means of rubber pinning and fiber bridge-over mechanisms [42].

Higher strain rate impacts were performed by using split Hopkinson Pressure Bar to obtain the dynamic compressive behavior of syntactic foams. Song, Chen and Frew [43] assessed that the compressive strength of epoxy syntactic foams increased with strain rate up to a transition strain rate between 550-1030s^{-1}.Woldesetbet and Peter [44] also studied the effects of volume fraction of syntactic foams on the strain rate properties. The results showed that there is a decrease in compressive strength and modulus for increasing volume fraction. For high strain rates of 800s^{-1}, there was a large decline in strength and modulus for up to 10-20% volume fraction followed by steady decline. Temperature effects on the dynamic compressive behavior were also studied by Song, Chen, Yanagita, and Frew [45]. Environmental temperature had a significant effect, i.e. with decreasing temperature, the foam initially hardens but then softens when below a transitional temperature. Based on the experimental data collected a model taking into account temperature and strain effects was developed and tested.

Hence even with the immense research in the field of strain rate testing on syntactic foams, there has not been much work that can be found for attenuation and wave speed of syntactic foams and FGMs. Not all sizes of microballoons have been tested for ultrasonic attenuation and wave speed measurements. There is also a lack of literature on the volume fraction FGMs material properties and layering effects. This study will focus on first developing a clear relationship of attenuation and wave speed behavior of syntactic foams with 3 different types of microballoons. This knowledge

will be utilized in making FGMs of different sized microballoons and characterizing them using ultrasonic techniques. Effect of radius ratio and volume fraction of syntactic foams on ultrasonic and compressive behaviors will also be studied. Future work will involve relating ultrasonic attenuation to stress wave attenuation from destructive impact testing.

References:

1. Mylavarapu, Phani, Woldesenbet, Eyassu, 'Ultrasonic Characterization of Sandwich Core Materials', Journal of Sandwich Structures and Materials 2008 10: 413-428

2. J.C. Drury, NDT FUNDAMENTALS: ultrasonics, part 7. The ultrasonic beam, *Insight* 47 (5) (2005), pp. 297–299

3. Kinra V K, Anand A.Wave propagation in a random particulate composite at Long and short wavelengths. Int J Solids Struct 1982; 18(5):367–80.

4. Song, Bo, Chen, Weinong, Frew, Danny J., Dynamic Compressive Response and Failure Behavior of an Epoxy Syntactic Foam, Journal of Composite Materials 2004 38: 915-936

5. Nikhil Gupta, Eyassu Woldesenbet, Patrick Mensah, Compression properties of syntactic foams: effect of cenosphere radius ratio and specimen aspect ratio, Composites Part A: Applied Science and Manufacturing, Volume 35, Issue 1, January 2004, Pages 103-111, ISSN 1359-835X

6. Biwa, S., Idekoba, S. and Ohno, N., 2002. Wave attenuation in particulate polymer composites: independent scattering/absorption analysis and comparison to measurements. Mech. Mater. 34, pp. 671–682

7. Phani Mylavarapu, Eyassu Woldesenbet, A predictive model for ultrasonic attenuation coefficient in particulate composites, Composites Part B: Engineering, Volume 41, Issue 1, January 2010, Pages 42-47, ISSN 1359-8368

8. Mouritz, A. P., Ultrasonic and Interlaminar Properties of Highly Porous Composites, Journal of Composite Materials 2000 34: 218-239

9. T. Hirone and T. Kamigaki, Attenuation of Ultrasonic Waves in Metals. I Aluminum, J. Japan Inst. Metals, 19 (1955),92
10. Ying C F, Truell R. 'Scattering of a plane longitudinal wave by a spherical Obstacle in an isotropically elastic solid'. J Appl Phys 1956; 27(9):1086–97.

11. Datta S K.,A self-consistent approach to multiple scattering by elastic Ellipsoidal inclusions, J Appl Mech 1977 ; 44 : 657–62.

12. Ishimaru, A.; , "Theory and application of wave propagation and scattering in random media," *Proceedings of the IEEE* , vol.65, no.7, pp. 1030- 1061, July 1977

13. Abraham I. Beltzer, Charles W. Bert, Alfred G. Striz, On wave propagation in random particulate composites, International Journal of Solids and Structures, Volume 19, Issue 9, 1983, Pages 785-791,

14. N. Brauner, A.I. Beltzer, Wave-obstacle interaction in a lossy medium: energy perturbations and negative extinction, Ultrasonics, Volume 26, Issue 6, November 1988, Pages 328-334,

15. Abraham I. Beltzer, Neima Brauner, The dynamic response of random composites by a causal differential method, Mechanics of Materials, Volume 6, Issue 4, December 1987, Pages 337-345,

16. A.I. Beltzer and N. Brauner, Acoustic waves in random discrete media via a differential scheme. *J. Appl. Phys.* **60** (1986), pp. 538–540.

17. Neima Brauner, Abraham I. Beltzer, The Kramers-Kronig relations method and wave propagation in porous elastic media, International Journal of Engineering Science, Volume 23, Issue 11, 1985, Pages 1151-1162

18. A. I. Beltzer and N. Brauner,*Waves of an arbitrary frequency in random fibrous composites*. J. Acoust. Soc. Am.*76*, No. 3, 962-963 (1984) (also XVI. Int. IUTAM Congress, Lyngby, Denmark, August 1984).

19. J. E. Gubernatis, E. Domany, Effects of microstructure on the speed and attenuation of elastic waves in porous materials, Wave Motion, Volume 6, Issue 6, November 1984, Pages 579-589

20. B.G. Martin, Ultrasonic attenuation due to voids in fibre-reinforced plastics, NDT International, Volume 9, Issue 5, October 1976, Pages 242-246

21. A.P. Mouritz, Ultrasonic & interlaminar properties of highly porous composites, *J Compos Mater* 34 (2000) (3), pp. 218–239.

22. J.M. Hale, J.N. Ashton, Ultrasonic attenuation in voided fibre-reinforced plastics, NDT International, Volume 21, Issue 5, October 1988, Pages 321-326
23. H. Jeong, Effects of Voids on the Mechanical Strength and Ultrasonic Attenuation of Laminated Composites *Journal of Composite Materials February 1997 31: 276-292*

24. S. Biwa, Y. Watanabe, S. Motogi, N. Ohno, Analysis of ultrasonic attenuation in particle-reinforced plastics by a differential scheme, Ultrasonics, Volume 43, Issue 1, October 2004, Pages 5-12

25. S. Biwa, Independent scattering and wave attenuation in viscoelastic composites, Mechanics of Materials, Volume 33, Issue 11, November 2001, Pages 635-647

26. S. Biwa, S. Idekoba, N. Ohno, Wave attenuation in particulate polymer composites: independent scattering/absorption analysis and comparison to measurements, Mechanics of Materials, Volume 34, Issue 10, October 2002, Pages 671-682

27. S. Biwa, Y. Watanabe, N. Ohno, Analysis of wave attenuation in unidirectional viscoelastic composites by a differential scheme, Composites Science and Technology, Volume 63, Issue 2, February 2003, Pages 237-247

28. S.M. Nair, D.K. Hsu, J.H. Rose, J. Nondestruct. Eval. **8**, 13 (1989)

29. I.M. Daniel, S.C. Wooh, I. Komsky, J. Nondestruct. Eval. **11**, 1 (1992)

30. V. Rajendran, N. Palanivelu, B.K. Chaudhuri, A device for the measurement of ultrasonic velocity and attenuation in solid materials under different thermal conditions, Measurement, Volume 38, Issue 3, October 2005, Pages 248-256

31. Christopher Layman, N. Sanjeeva Murthy, Ruey-Bin Yang, and Junru Wu, The interaction of ultrasound with particulate composites, J. Acoust. Soc. Am. 119, 1449 (2006)

32. Rohatgi, P. K., Matsunaga, T. and Gupta, N., Compressive and ultrasonic properties of polyester/fly ash composites. Journal of Materials Science, 2009. 44(6): p. 1485-1493.

33. E. Woldesenbet, N. Gupta and H. Jerro, Effect of microballoon radius ratio on syntactic foam core sandwich composites, *J Sandwich Struct Mater* **7** (2) (2005), pp. 95–111

34. Nikhil Gupta, Eyassu Woldesenbet, Patrick Mensah, Compression properties of syntactic foams: effect of cenosphere radius ratio and specimen aspect ratio, Composites Part A: Applied Science and Manufacturing, Volume 35, Issue 1, January 2004, Pages 103-111

35. Nikhil Gupta, Raymond Ye, Maurizio Porfiri, Comparison of tensile and compressive characteristics of vinyl ester/glass microballoon syntactic foams, Composites Part B: Engineering, Volume 41, Issue 3, April 2010, Pages 236-245

36. Nikhil Gupta, William Ricci, Comparison of compressive properties of layered syntactic foams having gradient in microballoon volume fraction and wall thickness, Materials Science and Engineering: A, Volume 427, Issues 1-2, 15 July 2006, Pages 331-342

37. Lorenzo Bardella, Francesco Genna, On the elastic behavior of syntactic foams, International Journal of Solids and Structures, Volume 38, Issues 40-41, October 2001, Pages 7235-7260

38. Rahul Jhaver, Hareesh Tippur, Processing, compression response and finite element modeling of syntactic foam based interpenetrating phase composite (IPC), Materials Science and Engineering: A, Volume 499, Issues 1-2, Fifth International Conference on Physical and Numerical Simulations of Material Processing (ICPNS 2007) held at Zhengzhou, China, October 23-27, 2007, 15 January 2009, Pages 507-517

39. J. R. M. d'Almeida, An analysis of the effect of the diameters of glass microspheres on the mechanical behavior of glass-microsphere/epoxy-matrix composites, Composites Science and Technology, Volume 59, Issue 14, November 1999, Pages 2087-2091

40. H. M. Hsiao, I. M. Daniel, Strain rate behavior of composite materials, Composites Part B: Engineering, Volume 29, Issue 5, September 1998, Pages 521-533

41. Eyassu Woldesenbet, Low velocity impact properties of nanoparticulate syntactic foams, Materials Science and Engineering: A, Volume 496, Issues 1-2, 25 November 2008, Pages 217-222

42. Guoqiang Li, Nji Jones, Development of rubberized syntactic foam, Composites Part A: Applied Science and Manufacturing, Volume 38, Issue 6, June 2007, Pages 1483-1492

43. B. Song, W. Chen and D.J. Frew, *J. Compos. Mater.* 38 (2004), pp. 915–936

44. E. Woldesenbet and S. Peter, Volume fraction effect on high strain rate properties of syntactic foam composites, *J Mater Sci* 40 (15) (2009), pp. 4009–4017.

45. Bo Song, Weinong Chen, Tamaki Yanagita, Danny J. Frew, Temperature effects on dynamic compressive behavior of an epoxy syntactic foam, Composite Structures, Volume 67, Issue 3, Dynamic Response of Advanced Materials and Structures, March 2005, Pages 289-298

CHAPTER 2

MATERIALS AND MATERIAL PREPARATION

2.1 Materials

2.1.1 Microballoons

Three types of soda-lime-borosilicate glass micro-balloon sizes with different outer and inner diameters were selected. The microballoons were manufactured by 3M under the brand name 'Scotchlite Glass Bubbles- General Purpose Series' [1]. The details about the microballoons are provided in Table 1.

Radius ratio is defined as the ratio of inner and outer radius of the sphere and represents the hollowness of the sphere. The spheres have different radius ratio and size leading to difference in density and void content in epoxy syntactic foam. As the radius ratio and particle size increases the density of the syntactic foam for the same volume fraction decreases. The density of the syntactic foams also decreases with increase in volume fraction due to increasing voids inside the matrix.

Table 1. Microballoon properties

Microballoon Type	Average Particle size (µm)	Density of Particle (kg/m^3)	Crush Strength (90% survival, Mpa)	Average Wall thickness (µm)	Radius Ratio (r_i/r_o)
S60/10000	30	600	68.94	1.49	0.950
K37	45	370	20.68	1.04	0.977
K1	65	125	1.72	0.55	0.992

2.1.2 Virgin Epoxy

The epoxy used for making all samples was Epo-Thin resin and hardener manufactured by Buehler, Ltd [Appendix C]. The primary composition of the epoxy resin is Bisphenol –A type (60-100%) by weight and its identification is Buehler ID 20-8140-128. The hardener's primary composition is Polyoxyalkylamine (30-60%) by weight and its identification is Buehler ID 20-8142-064. The manufacturer specified density is 1147 kg/m^3.

2.2 Material Preparation

2.2.1 Syntactic Foams

Appropriate amounts of resin and hardener were poured according to the manufacturers specifications. The epoxy was mixed in the ratio of 73.5% resin and 26.4% hardener.

First, hardener was poured in a heat resistant paper cup and weighed in a OHAUS Scout Pro digital scale with an accuracy and maximum weight limit of 0.1g and 400g, respectively. The required amount of resin was poured into the cup which was tilted at a 45 degree angle and gently stirred using a wooden stirrer. After 5 minutes of stirring, the cup is left alone at room temperature for another 5 minutes to reduce the amount of air bubbles formed during stirring.

The cup is then placed back into the scale and a known mass of microballoons is added to the mixture. It is stirred again slowly until all the clumps of microballoons have been dispersed evenly in the mixture. It is then cast into 1.5" (38.1 mm) inner diameter and 1" (25.4 mm) inner height plastic cylindrical casting cups (manufactured

by Beuhler, ID 20-9181). These cups have been coated with release agent (Beuhler ID 20-8185-016), 5 minutes prior to pouring the mixture so that the epoxy will not bond to the walls upon hardening.

After pouring the mixture into the cup it is taken to a vacuum chamber and kept at a vacuum pressure of 30 torr (0.58 psi) for 10 minutes to remove air bubbles. It is then gently stirred and set to cure for 24 hours at room temperature although a set time of 9 hrs is specified by manufacturer. Due to the microballoons having lower density than the surrounding epoxy, it rises up through the mixture during the vacuuming process. Hence the mixture is gently stirred again before setting it for cure.

After curing the sample is extracted from the casting cup and machined to the required size for testing.

2.2.2 Functionally Graded Syntactic Foams (FGMs)

The cast is assembled and labeled with a marks for each layer as shown in Figure 1. For making a 0-40% 5 layered FGM specimen the cast is first set on top of flat base of lexan sheet of 0.5" (12.7 mm) thickness. Lexan is used here since it can withstand the high temperature exothermic reaction taking place during the casting of the syntactic foam mixture and is transparent. The front and back sheets of the casting mold are also made of Lexan, whereas the side plates are made from T-6061 grade Aluminum. The mold is sealed around with plastilina modeling clay manufactured by Sculpture House, Inc.

After the cast has been placed, the first layer from the bottom is filled with of virgin epoxy and left to cure for 1 hour. After another hour 10% volume fraction syntactic foam mixture is poured on top of the first layer until it reaches the location

designated for the bottom of 3rd layer. Here no adhesive is added as the bond between the layers is assumed to be stronger and a more linear variation of the gradation is obtained. This process continues with increasing volume fraction upto a 40% volume fraction at the top of the cast. The top layer has slightly larger thickness so that it is easier to machine to the required dimension for testing. The same process is followed for making 0-30% FGM.

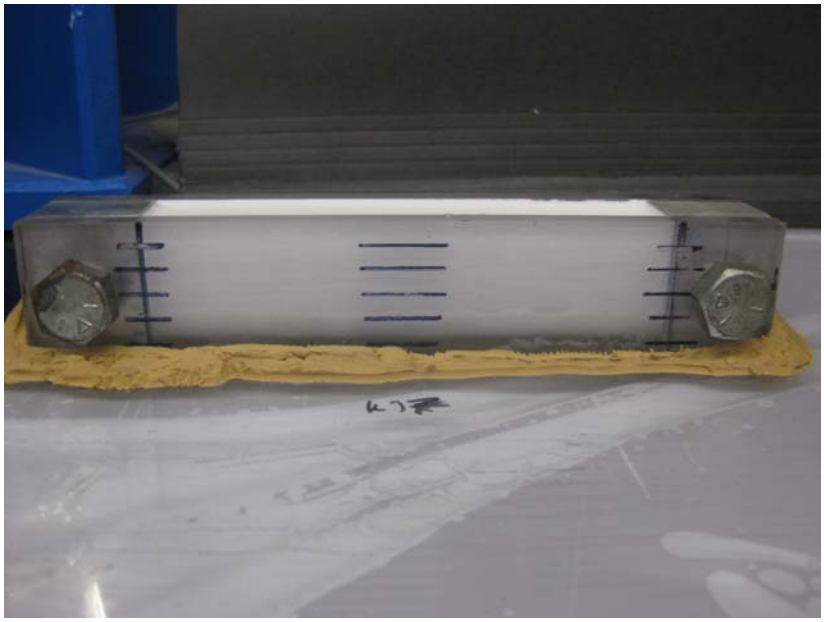

Figure 1. Casting Mold for Preparation of FGMs

2.3 Volume Fraction and Density Calculation

In order to characterize the volume fractions and the required mass of microballoons in the syntactic foam, Equation 1 was used. Volume fractions ranging from 5-40 % were calculated in this analysis. Table 2 shows the syntactic foam composition by mass for one casting cup.

$$V_f = \frac{\frac{m_s}{\rho_s}}{\frac{m_s}{\rho_s} + \frac{m_e}{\rho_e}} \quad [1]$$

Where m_s = mass of sphere (kg)

ρ_s = density of sphere (kg/m^3)

m_e = mass of epoxy (kg)

ρ_e = density of epoxy (kg/m^3)

Table 2. Syntactic Foam Composition by Mass for 1 Casting Cup

Sample	Volume Fraction	Mass of Microballoons (g)	Mass of Hardener (g)	Mass of Resin (g)
S-60	5%	0.5	4.5	12.5
	10%	1.0	4.5	12.5
	20%	2.2	4.5	12.5
	30%	3.8	4.5	12.5
	40%	5.9	4.5	12.5
K-37	5%	0.3	4.5	12.5
	10%	0.6	4.5	12.5
	20%	1.4	4.5	12.5
	30%	2.4	4.5	12.5
	40%	3.7	4.5	12.5
K-1	5%	0.1	4.5	12.5
	10%	0.2	4.5	12.5
	20%	0.5	4.5	12.5
	30%	0.8	4.5	12.5
	40%	1.2	4.5	12.5

Density was calculated from the measured dimensions and weight of all the specimens. For a particular volume fraction, six specimens of Syntactic foams 1" (25.4 mm) diameter and 0.5" (12.7 mm) thickness were measured and their corresponding weight were also measured. For FGM 0-40%, 6 specimens of 1 x 1x 1 inch (25.4 x 25.4 x 25.4 mm) and their corresponding weight was measured. For FGM 0-30%, 6

specimens of 1 x 1 x 0.8 inch (25.4 x 25.4 x 20.3 mm) and their corresponding weight was measured. Results of density calculation of fabricated syntactic foams are shown in Figure 2. Results of density calculation of FGMs are shown in Figure 3 and Figure 4. As shown in Figure 2, the measured density decreases with increasing volume fraction. Also from Figure 3 and 4, the measured density of FGMs decreases for increasing microballoon size.

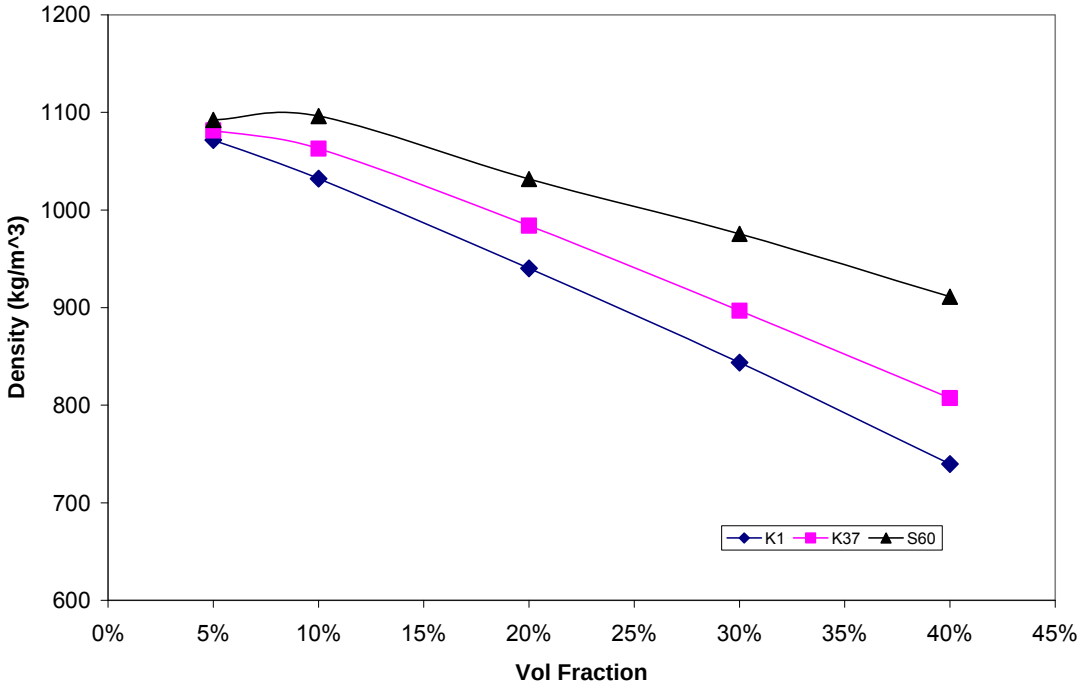

Figure 2. Measured density of Syntactic foams of varying volume fractions

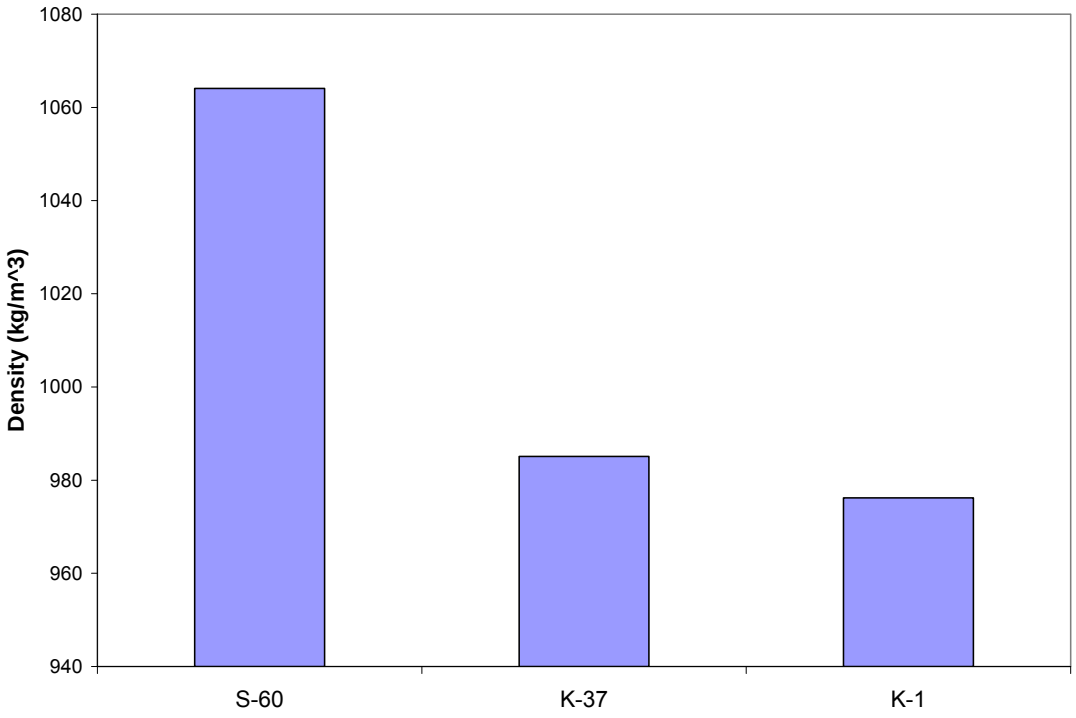

Figure 3. Measured density of FGMs of 0-40% of varying volume fractions

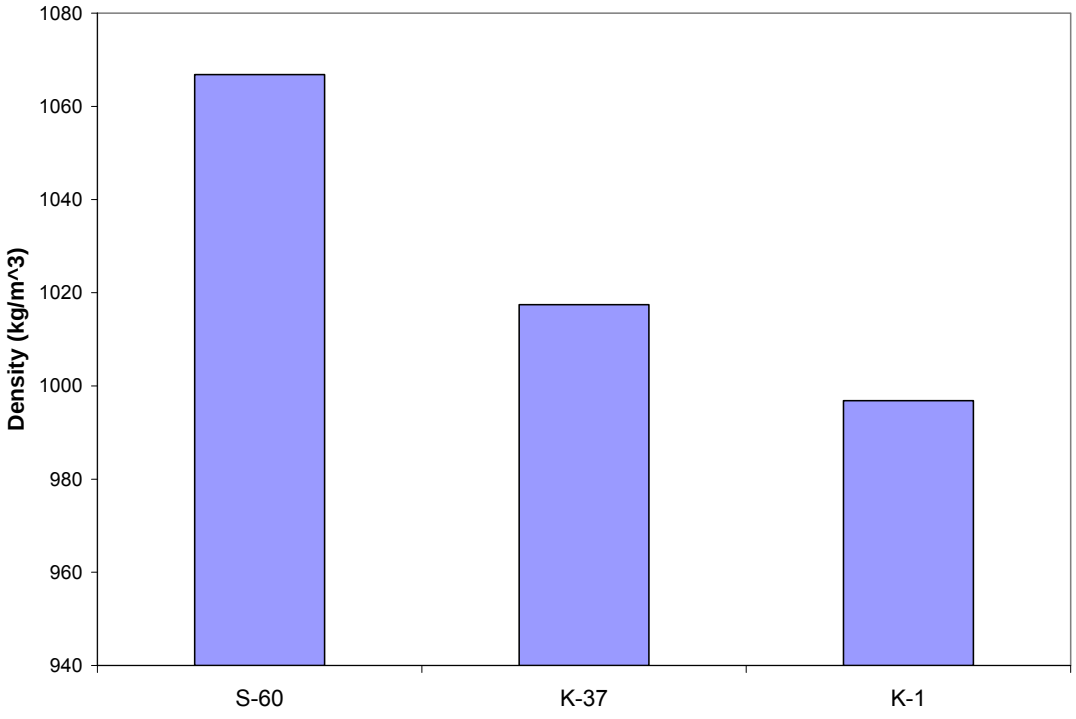

Figure 4. Measured density of FGMs of 0-30% of varying volume fractions

The values of density are higher for the FGMs 0-30% than the FGMs 0-40% because with increasing layer of higher volume fraction, more voids are created and hence it lowers the overall density of the FGM. It is assumed for all analysis that, the volume fraction of natural voids, formed during the mixing and curing process is negligible and occupies 0 to 4% with the latter value being for higher volume fractions.

References:

1. www.3m.com, 3M™ Microspheres Selection Guide. (2009). Retrieved April 11, 2009, from, http://multimedia.3m.com/mws/mediawebserver?mwsId=66666UuZjcFSLXTtlXM6LxfXEVuQEcuZgVs6EVs6E666666--&fn=MicroSelectGuide_DMR.pdf

CHAPTER 3

EXPERIMENTAL PROCEDURES

3.1 Ultrasonic Testing

The main focus of this study was to characterize the syntactic foams according to ultrasonic wave speed and attenuation. All specimen faces were sandpapered to make the surfaces smooth for ultrasonic testing. Description of the experimental setup, equipments used, instrumentation, test procedure and data analysis for the ultrasonic tests are given below. Figure 5 gives the overall view of the experimental setup used for immersion testing.

3.1.1 Experimental Setup

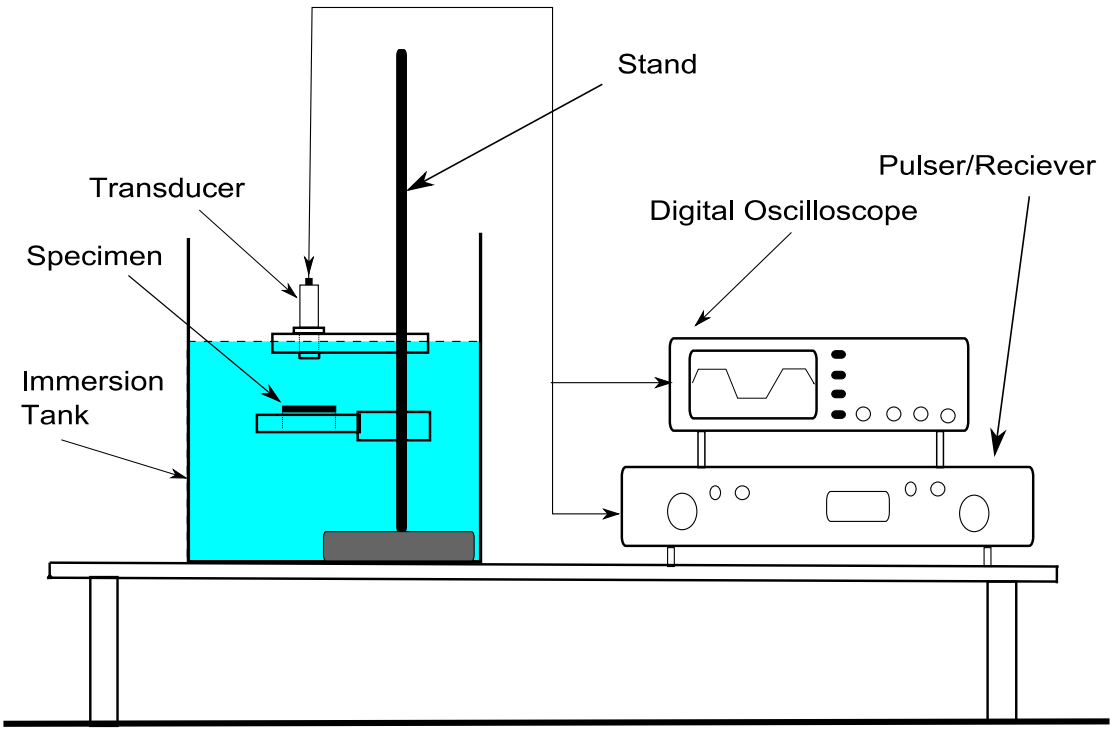

Figure 5. Ultrasonic Immersion Testing Setup

Here the pulser/receiver instrument generates short, large amplitude electric pulses that are converted into short ultrasonic pulses that are applied to the ultrasonic transducer. The pulses cause the piezo-electric crystals to vibrate and thus produce an ultrasonic wave.

The wave from the transducer travels through the specimen and the voltage signals from the reflected waves at the back surface of the specimen are detected, amplified and measured in the oscilloscope. The reflection happens at the back surface and the front surface due to the large impedance mismatch between the solid specimen and water (couplant). Both surfaces of the specimen are exposed to water for uniform coupling which reduces the sensitivity variations of the received signal for immersion transducers. A thick, sticky and highly viscous PANAMETRICS couplant SWC was used for shear wave contact transducers for shear wave testing as shear waves does not propagate in liquids.

3.1.2 Equipment Used:

Transducers

Ultrasonic tests were carried out with both immersion and contact type transducers. The transducers used for the test were of the frequency 1 MHz for immersion and 2.25 MHz for shear wave contact testing. Higher frequency immersion transducers from 2.25 to 5 MHz were neglected for the test due to the high attenuation and inconsistent results. All samples were tested using pulse-echo method to determine the response to ultrasonic waves.

The longitudinal wave attenuation and wave speed were evaluated using the ultrasonic immersion transducer as shown in Figure 6. The shear wave speed was measured using the contact transducer as shown in Figure 7.

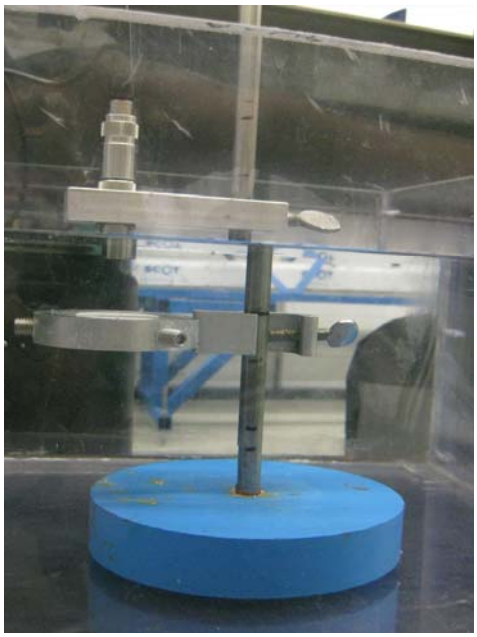

Figure 6. Longitudinal wave immersion transducer

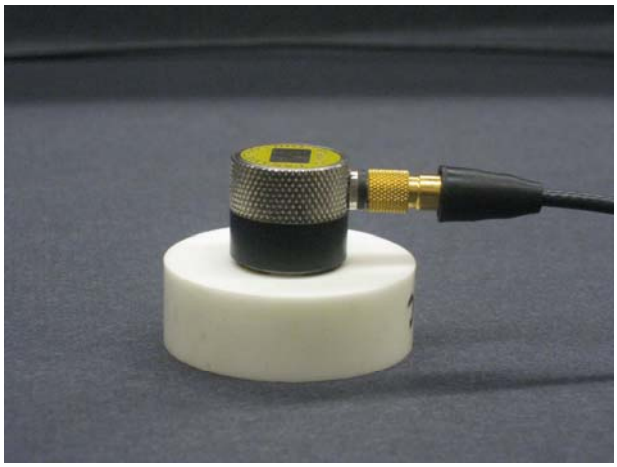

Figure 7. Shear Wave Contact Transducer

Both immersion and shear ultrasonic transducers had a diameter of 0.5" (12.7 mm). The near field distance or water path of 26.5 mm was chosen for the immersion

testing. An average of 16 values was taken for each waveform passing through a point in the oscilloscope. The gain was set such that at least 2 back reflections were seen during the event. All tests were carried in water and of a room temperature of 23 degree Celsius. Calibration of the transducers was done for materials with known wave speeds (aluminum and polycarbonate) before each test to ensure the correctness of the experimental results.

Pulser/Reciever

The pulser/receiver unit for all the ultrasonic testing was the PANAMETRICS 5058 –PR as shown in Figure 8. It was designed specifically for a pulse-echo or through transmission testing modes but only the former was used here. It has a capability of excitation voltages of up to 900 V. It has up to 80 dB of attenuation and 60 dB of gain for signals entering the receiver unit. The high voltage pulser and high gain receiver make it ideal for testing composites. Signals received by the receiver unit are transmitted to the oscilloscope for further processing.

Figure 8. Panametrics Pulser/Reciever 5058 PR unit

Digital Oscilloscope

A Tektronix TDS 3014B Four Channel Color Digital phosphor oscilloscope capable of 10000 sample points per second was used as shown in Figure 9. The BNC end of the coaxial cable was attached to the Rf connecter of the pulser/amplifier. The scale on the oscilloscope was 4 μs/div on the X axis and 1 Volt/div on the Y axis. The data was saved in a 3.5" (88.9 mm) floppy disc and transferred to the computer for further analysis.

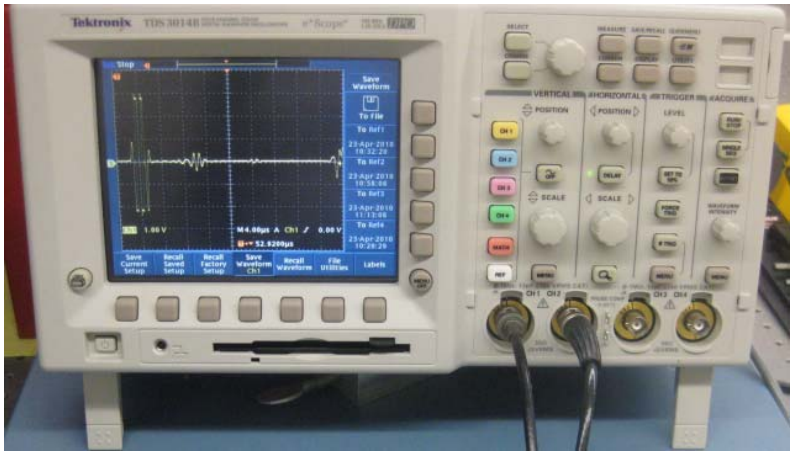

Figure 9. Digital Oscilloscope for Wave detection

Tank and Accessories

The immersion tank is made up of 0.5" (12.7 mm) thick polycarbonate sheets. The stand is stainless steel and the specimen and transducer holders were made with T-6061 grade aluminum. It was chosen as it was easily machinable and non-corrosive. Rubber gaskets were inserted in between the insertion of transducers to allow for proper parallel alignment with the specimen and loss of signal from contact with the aluminum periphery. A level was used to check the alignment before experimentation. The coaxial cable of 50 ohm impedance with a BNC to waterproof UHF (up to 50m)

was used for the immersion testing. The shear wave testing was conducted with a 50 ohm coaxial cables with BNC to microdot connecters.

3.1.3 Test Procedure

Immersion Testing

1. Fill the tank with water up to 7.5” (190.5 mm) depth and water temperature of 23º C.
2. Connect the BNC Cable output to the receiver and the UHF output to the transducer.
3. Connect the BNC cable from the sync out from pulser/receiver to the oscilloscope Channel 2.
4. Connect the BNC cable from the RF output of the pulser/receiver to the oscilloscope Channel 1 as shown in Figure 10.

Figure 10. Cable connection of Pulser/Reciever and oscilloscope

5. Turn on Oscilloscope and set the Y axis as 1volts/div, X axis to 4μs/div and from the 'Acquire Menu' select mode and set to 16 point averaging.
6. Set the Pulser/Receiver settings to repetition rate of 500 Hz, damping to 200Ω, pulse height to 200 volts, mode to pulse echo transmission, attenuation to 0 dB, gain to 40 dB, HP filter to 1 MHz, LP filter to out.
7. After machining to the required dimensions, the prepared specimen's center was located and 0.5" (12.7 mm) circle was drawn around it with a circular ruler as shown in Figure 11. The required measurement of height of specimen was measured from the center of the circle with a micrometer with 0.0001" (0.00254 mm) precision.

Figure 11. Circular Ruler Marking

8. It is then placed on the specimen holder and tightened with the help of 3 soft tip set screws at 120 degrees angle around the periphery as seen in Figure 12.

The specimen holder is then slid on the stand until it reaches the tip of the transducer.

9. The specimen holder screw was tightened at the end of clamp. Alignment of the circle of specimen to the tip of transducer was done by slightly pressing the specimen against the transducer bottom with a flat plate. The soft tip screws were loosened and slight adjustments were made. They were tightened again, ensuring the transducer and the circle drawn on the specimen were vertically aligned.

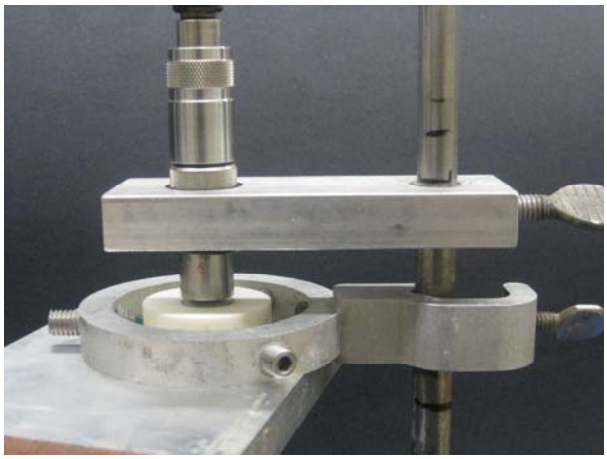

Figure 12. Aligning of Specimen with transducer

10. The specimen holder screw was loosened and slid against the stand until it reached a position corresponding to a distance of 1.1” (27.9 mm) between the specimen’s top face and the transducer. It was then tightly screwed as shown in Figure 12.
11. The whole setup was immersed in water and the pulser/amplifier turned on.

12. Disturbances in water were allowed to subside and the data was recorded by the oscilloscope.
13. The specimen was removed steps 7-12 were, again, repeated.

Shear Wave Testing

1. Connect the BNC Cable output to the receiver and the Microdot output to the transducer.
2. Connect the BNC cable from the sync out from pulser/receiver to oscilloscope Channel 2.
3. Connect the BNC cable from RF output from pulser/receiver to oscilloscope Channel 1.
4. Turn on Oscilloscope and set the Y axis as 1 volt/div, X axis to 4μs/div and from the 'Acquire Menu' select mode and set to 16 point averaging.
5. Set the Pulser/Reciever settings to repetition rate of 200 Hz, damping to 500Ω, pulse height to 400 volts, Mode to pulse echo transmission, Attenuation to 21 dB, Gain to 40 dB, HP filter to 1 MHz, LP filter to out.
6. Place SWC couplant around the circle of specimen and place specimen on top of a flat, hard surface.
7. Press the shear wave transducer gently against the couplant layer.
8. Turn on the pulser/receiver and save the data in oscilloscope.
9. Repeat steps 6-9.

3.2 Compression Testing

For further characterization of syntactic foams and graded materials, quasi-static tests were conducted using ASTM D 695-63T Standards [1]. The tests were conducted in an Instron 5582 machine with a loading speed of 1.3mm/min. The force measuring range of the load cell is from 0-100 kN which is applicable for this study. The tests were conducted until total fracture of the specimens, as seen from the real-time load extension graphs on the computer connected to the Instron machine. The data was obtained from the load transducers attached to the Instron head. After completion of the experiment, the data was analyzed and plotted to evaluate true stress-strain plots. Specimens were coated on the top and bottom surface with a thin layer of lubricant for better contact between machine head and specimen. Before running the tests, a compliance test at 0.01in/min (0.254 mm/min) with no sample was conducted for calibration of the initial adjustments of machine head. Figure 13 shows the Instron testing machine used for quasi static testing.

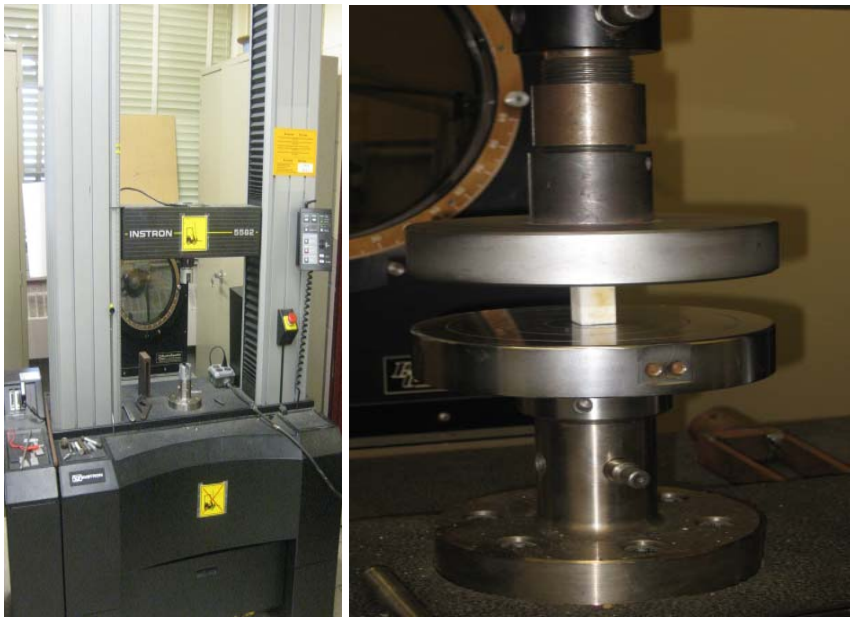

Figure 13. Instron Machine with compression head

3.3 Drop Tower Impact Machine

A Dynatup 9210 drop tower assembly was used for low velocity impact at 3 m/s impact velocity as shown in Figure 14. The impact data which includes the load, energy, displacement, velocities with respect to time is obtained by the data acquisition software connected to the drop tower assembly.

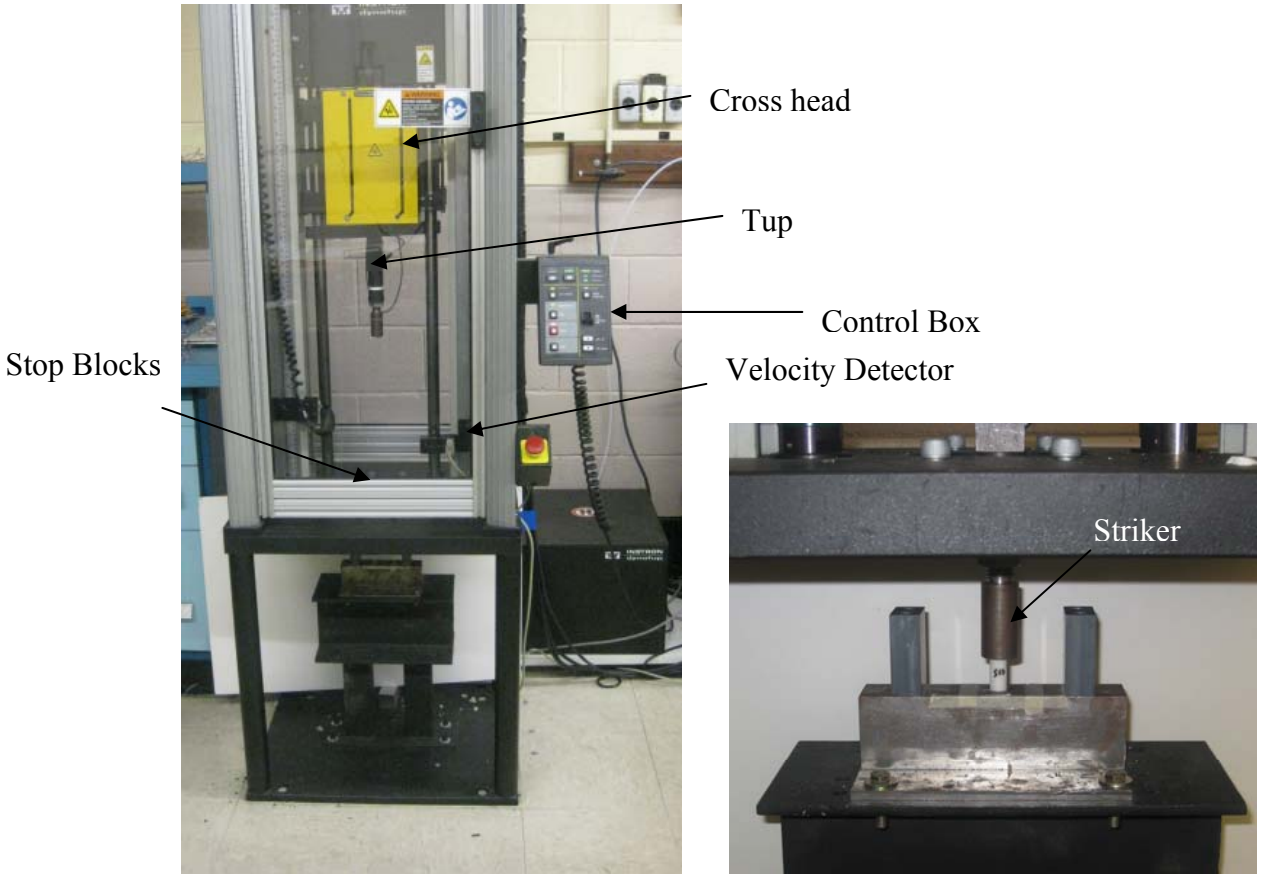

Figure 14. Left: Instron Dynatup 9210 drop tower. Right: Fixed back fixture

The system is capable of producing impact velocities up to 5m/s depending upon the weight and height input into the system. Various types of strikers can be adjusted into the tup which records data up to maximum load of 10,000lb (44.48 kN). The sampling rate of the system is up to 4.1 MHz. The system was modified to allow

for the implementation of a fixed back support fixture outside the drop tower enclosure. The impact test was performed until the bottom of the cross head reaches the stop blocks.

First the drop height was that would result in an impact velocity of 3m/s must be determined. The mass of the system was first calculated. It included the total mass of crosshead, weights, tup, tup bolts, striker, reaction plate and bolts. Table 3 shows all the components of mass being applied to the system.

Table 3. Total mass of drop weight

Components	Reaction plate and bolts	Tup and Bolt	1"(25.4 mm) flat striker	Cross Head	Weights	Total Mass
Mass(kg)	1.39	0.85	0.29	4.79	5.22	12.54

A height of 48.5 cm was chosen after repeated calibration velocity tests at different heights to obtain the impact velocity of 3m/s. 60J of impact energy was imparted to the specimen. The impact energy for the analysis was determined by,

$$E = mgh \qquad [2]$$

Where m is the total mass of the drop weight, g is the acceleration due to gravity and h is the height from which the mass was dropped.

Also verification of the impact velocity obtained from machine was checked against velocity determined by

$$v = \sqrt{2gh} \qquad [3]$$

When checking the velocity of impact, first the striker bar is lowered until it just touches the specimen. Then the velocity sensor is adjusted so that the bottom edge

of the detector aligns with the bottom edge of the flag. This is the point from which the height is calculated for testing. A number of velocity tests are performed before each set of experiment. A quoted calibration factor was input for the tup for correct data acquisition. The input variables are listed in Table 4.

Table 4. Tup calibration

Signal Source	Filter (kHz)	Max Load (kN)	Tup calibration factor (kN)	Load Range (kN)
Tup	4	44.482	38.939	44.482

The duration of data collection was set at 20 ms at a sampling rate of 409.6 kHz to allow ample time of data recording during the impact event. The impact time was between 0.5 to 6ms.

References:

1. ASTM D-695-85, "Standard Test Method for Compressive Properties of Rigid Plastics," pp. 199-204, 1988

CHAPTER 4

RESULTS AND DISCUSSIONS

4.1 Ultrasonic Tests

4.1.1 Ultrasonic Testing of Syntactic Foams

In a transducer there are many waves that emanate from the piezo-electric element face which transmits vibration through the electrostriction of piezo-electric crystals. It results in sound field interacting or interfering with each other and superimposition of sound pressure or interaction of sum of amplitudes of individual waves as the wave propagates out in a circular wavefront. The interaction points are known as nodes and antinodes. At the face of the transducer there are extensive nodes and it is called near field zone. This beam spreads out and a far field zone of intense uniform field develops at a certain distance from transducer field. This far field zone is the ultrasonic longitudinal wave travelling through a medium. For our ultrasonic testing we utilize the propagation of this longitudinal wave using the C scan method.

In a typical C-scan ultrasonic pulse echo technique acoustic impedance plays a major role in analyzing the wave data. Acoustic impedance (Z) of a material is defined as [1, 2]:

$$Z = \rho \bullet v \qquad [4]$$

Where ρ is the density of the material and v is the sound velocity. At the boundary between two materials lies the acoustic interface where, due to different acoustic impedance of the two materials, a wave travelling from one media to another

is partially transmitted and partially reflected as shown in Figure 15. According to Non-Destructive Testing (NDT) [3] the reflection coefficient (R) is calculated by:

$$R = \left(\frac{Z_2 - Z_1}{Z_2 + Z_1} \right)^2 \quad [5]$$

$$T = 1 - R \quad [6]$$

Where T is the transmission coefficient. The amount of energy reflected depends upon the difference in acoustic impedances at the boundary. The higher the difference in acoustic impedances, the higher will the value of the reflection coefficient be. Hence this property determines the wave energy being reflected from the interface boundary.

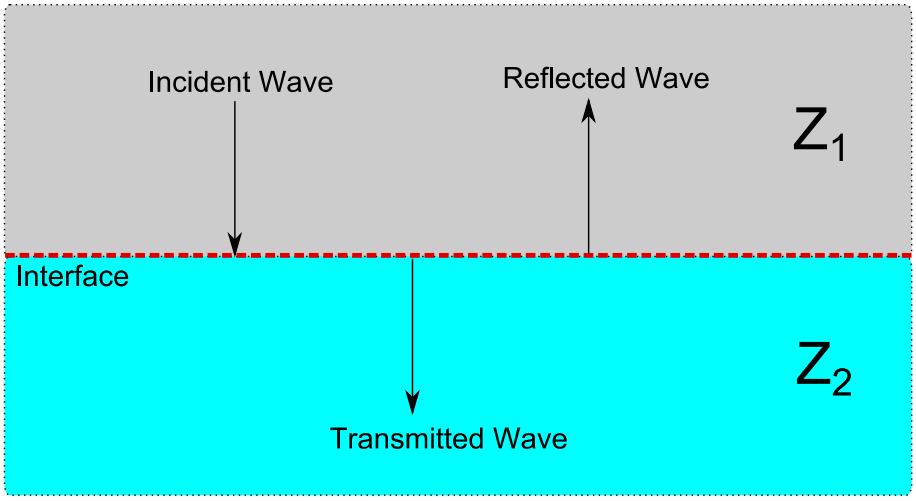

Figure 15. View of reflected and transmitted wave at interface boundary

A typical ultrasonic wave form obtained for the syntactic foams is shown in Figure 16. The peaks corresponding to the back wall reflection of the specimen can be clearly seen from Figure 16. The location in the time axis and the corresponding amplitude is noted for the first two back wall reflections to calculate the longitudinal wave speed and attenuation in the specimen. The third back wall reflection was

omitted because it could not be detected in all samples. ASTM E664 –93 is used to calculate the apparent attenuation [4].

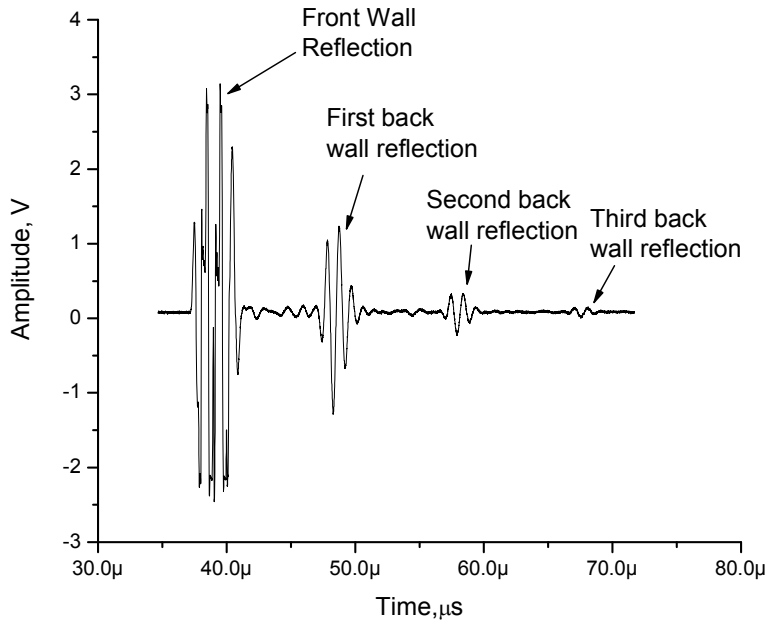

Figure 16. A typical syntactic foam Ultrasonic pulse-echo response

The apparent attenuation coefficient is calculated by the Equation [7].

$$\text{Apparent attenuation} = \frac{20 \times \log_{10} \frac{A_m}{A_n}}{2(n-m)t} \qquad [7]$$

Where A_m and A_n = amplitude of m^{th} and n^{th} back reflections ($n>m$) and t = specimen thickness.

Attenuation of an ultrasonic wave here is compared with a previously determined theoretical model for low volume fractions. The model, developed by Mylavarapu and Woldesenbet [5] is based on ultrasonic attenuation by scattering and absorption of spherical elastic microballoons taking into account the matrix

attenuation. Their model takes into account the effect of particle size, porosity and radius ratio. Attenuation coefficient according to model proposed by Mylavarapu and Woldesenbet is calculated by Equation 8 [5].

$$\alpha_{Comp} = \alpha_{Epoxy} + \frac{-1}{4l}\ln\left(1 - \frac{3 * V_f * l}{4 * \pi * r^3} * (\gamma_s + \gamma_a)\right) \quad [8]$$

Where α_{Epoxy} = attenuation by pure epoxy

V_f = Volume Fraction of microballoons (0-30%)

l = length of the specimen (m)

r = microballoon outer radius (m)

γ_s= scattering coefficient

γ_a= absorption coefficient

The attenuation calculated by Equation 8 takes into account the attenuation of pure epoxy samples measured experimentally. Also the wave speeds from experiments are used to calculate the scattering and absorption of the hollow microballoons.

The longitudinal wave speed was calculated according to the time lag between the first two back wall reflections and the peaks associated with it, in immersion pulse echo testing. The shear wave speed was calculated using first two back wall reflections in contact type pulse echo testing. The longitudinal (V_l) and shear (V_s) velocities in (m/s) can be computed by Equations [9a-9b]

$$V_l = \frac{2t}{T_l} \quad [9a]$$

$$V_s = \frac{2t}{T_s} \quad [9b]$$

Where T_l and T_s are time of flight of longitudinal and shear wave and t is the specimen thickness. Attenuation and wave speed were processed from the raw data obtained from the experiment.

Further characterization of syntactic foams is done by calculation of Young's modulus, shear modulus and Poisson ratio. An assumption is made here that the material being tested is linear elastic isotropic solid and the equations for determining the material properties are valid for one dimensional wave theory. This assumption is based on the fact that during mixing the microballoons were evenly mixed with the epoxy in all directions, thus the wave speed will be the same in all directions. Wave speeds were evaluated at frequencies of 1 MHz for longitudinal and 2.25 MHz for shear wave speed measurement. Equations 10-12 are used to calculate the material parameters [2]:

$$\nu = \frac{1 - 2(V_s / V_l)^2}{2 - 2(V_s / V_l)^2} \qquad [10]$$

$$E = \frac{V_l^{\,2} \nu (1 + \nu)(1 - 2\nu)}{1 - \nu} \qquad [11]$$

$$G = V_s^{\,2} \nu \qquad [12]$$

Where ν is the Poisson ratio, E is the Young's Modulus and G is the shear modulus.

Specimens' sizes for all syntactic foam testing were 0.5" (12.7 mm) thickness and 1.5" (38.1 mm) diameter. Five specimens were tested per volume fraction for all syntactic foams. The water path between the transducer and the specimen was 26.5 mm.

Attenuation results

Attenuation coefficient for pure epoxy was 0.434 dB/mm. All errors are calculated by taking the change from the mean value, the maximum and minimum from the five samples. Some examples of wave reflections obtained from the syntactic foams are shown in Figures 17-19.

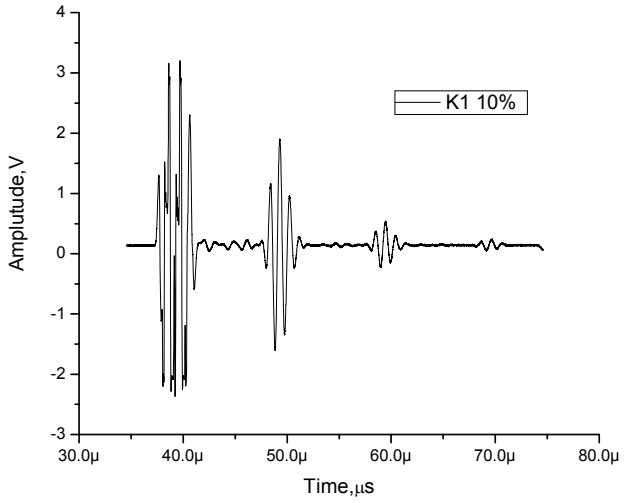

Figure 17. Amplitude vs. Time plot of K1-10 sample

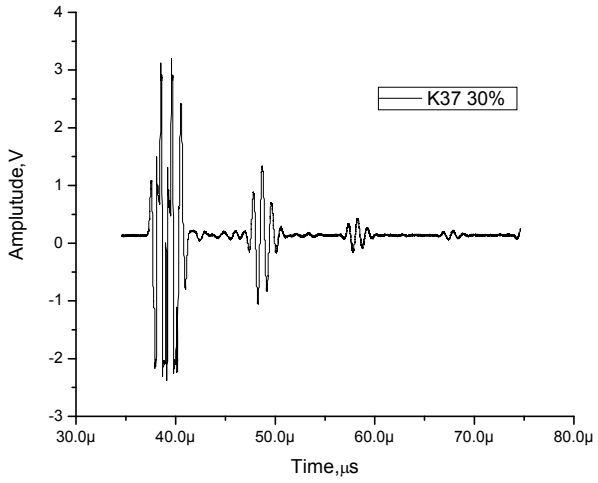

Figure 18. Amplitude vs. Time plot of K37-30 sample

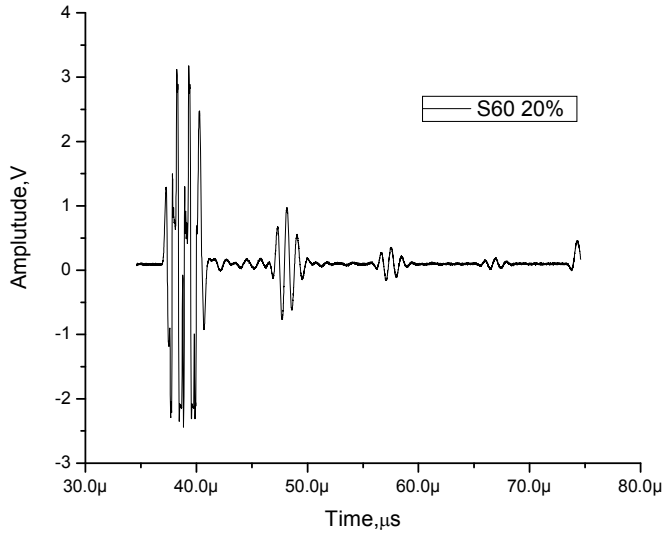

Figure 19. Amplitude vs. Time plot of S60-20 sample

Attenuation coefficient calculated for volume fractions of 0-30% for the different types of syntactic foams are plotted on the Figure 20. As seen from Figure 20 and Table 5, attenuation is highest for the largest size micro-balloon (K1) and lowest for smallest size microballoon S60. It increases for increasing volume fractions for K1 and decreases for K37 and S60 size microballoons.

Table 5. Attenuation coefficient values with error

1 MHz Attenuation	Epoxy (T) (dB/mm)	K1 (dB/mm)	K37 (dB/mm)	S60 (dB/mm)
5%	0.434	0.457± 0.040	0.394± 0.010	0.379 ± 0.030
10%	0.434	0.480± 0.045	0.389± 0.021	0.357± 0.033
20%	0.434	0.541± 0.033	0.360± 0.036	0.340± 0.022
30%	0.434	0.632± 0.029	0.363± 0.018	0.324± 0.021

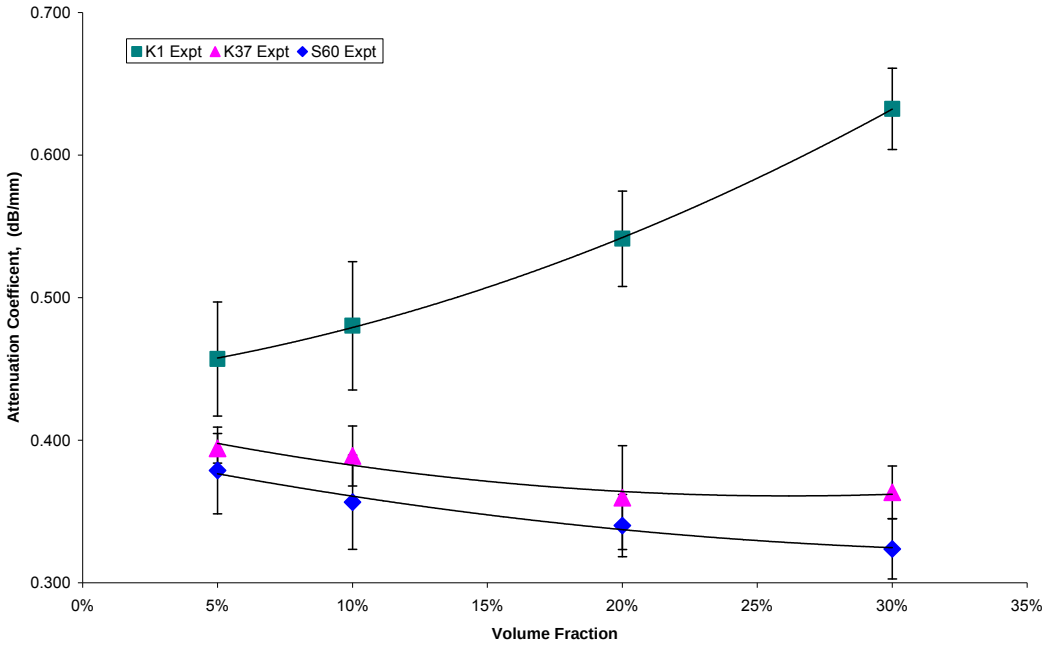

Figure 20. Attenuation coefficient calculated from syntactic foams

In syntactic foam composites, wave propagation behavior, such as scattering at inclusions governs the elastic properties obtained by ultrasonic testing and are determined by the ratio of wavelength to particle size [6]. The range of the wavelength to particle size ratio was between 35-92 at 1 MHz as shown in Table 6. Hence, the ultrasonic wave will pass through clusters rather than millions of particles that are present in the composite. Therefore, scattering of ultrasonic wave does not occur at each and every particle–particle interface rather than between clusters of particles [6]. Due to the ratio being smaller for K1 size sphere than the S60 and K37, there is more probability of wave-particle interaction to occur hence a case for increase in wave attenuation. Due to the larger voids and smaller wall thickness, K1 size microballoon interacts with the plane longitudinal wave causing more scattering and absorption. It

can further be noted that as the radius ratio decreases the material becomes more elastic, the absorption cross-section becomes zero and does not contribute to wave decay [7]. Hence the attenuation of K37 microballoon is higher than S60 due to larger voids for the same volume fraction and higher density.

Table 6. Ratio of wavelength to microballoon size at 1 MHz

Type	Volume Fraction of Sample	Ratio of wavelength to particle size for 1 MHz
S60	5%	85.97
	10%	86.74
	15%	87.60
	20%	89.62
	25%	91.15
	30%	91.80
K37	5%	56.72
	10%	57.24
	15%	57.68
	20%	57.20
	25%	58.02
	30%	58.60
K1	5%	38.85
	10%	38.23
	15%	37.72
	20%	36.96
	25%	36.46
	30%	35.96

Longitudinal wave speeds of syntactic foams are shown in Figure 21. It can be seen that the wave speed increases with volume fraction for S60 and K37 type syntactic foams whereas it decreases for K1 type syntactic foams. Because of the larger voids and smaller wall thickness, K1 size microballoons interact with the plane longitudinal wave causing more scattering and absorption. The longitudinal velocity also decreases with increasing volume fraction due to more wave interaction with microballoons as shown in Figure 21. An increase in wave speed is the result of the

wave travelling faster in the microballoon of smaller sizes S60 and K37 than the epoxy matrix hence less interaction with the surrounding particles and less scattering. Average longitudinal wave speed values were calculated from 5 samples for each type of syntactic foam.

All longitudinal wave speed values for the syntactic foams with S60 and K37 were higher than pure epoxy longitudinal wave speed which was 2526 m/s. The small drop in wave speed for K37 at 20% volume fraction was negligible and could be due to properties of wave propagation not varying for low volume fractions in the range of 10-20%.

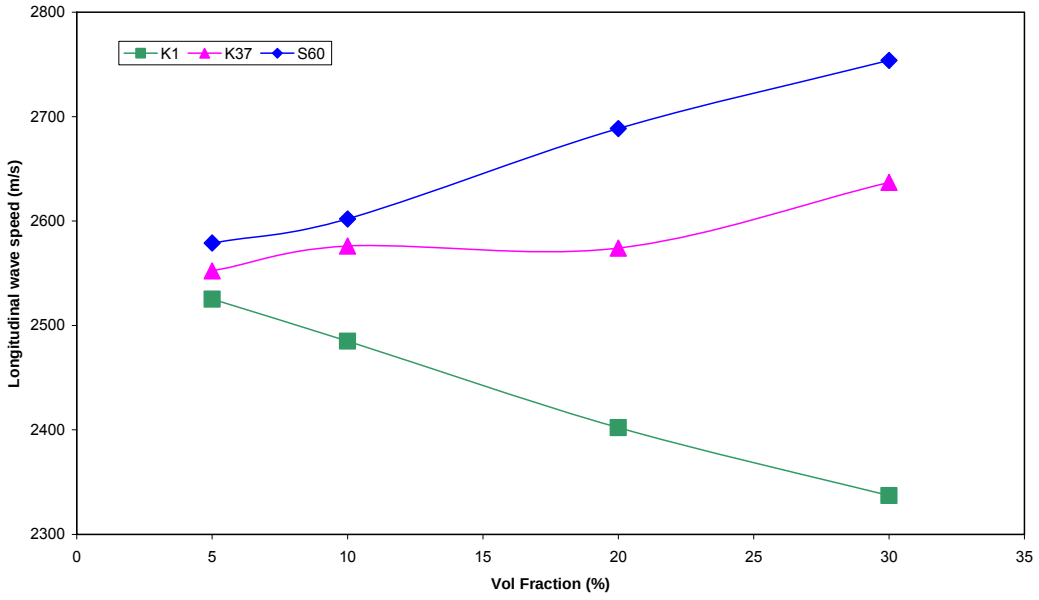

Figure 21. Longitudinal Wave Speed of Syntactic Foams

Shear wave speed measurements are shown in Figure 22 for all syntactic foams up to 30% volume fraction. Shear wave speed is generally smaller than the

longitudinal wave speed due to shear waves travelling parallel to wave propagation and have weaker energy. Also there is less interaction between shear waves with microballoons during wave propagation due to motion of wave travel. Similar trends as the longitudinal wave speed was seen with shear waves. Wave speed of K37 and S60 increased with increasing volume fractions and wave speed of K1 decreased slightly with increasing volume fractions.

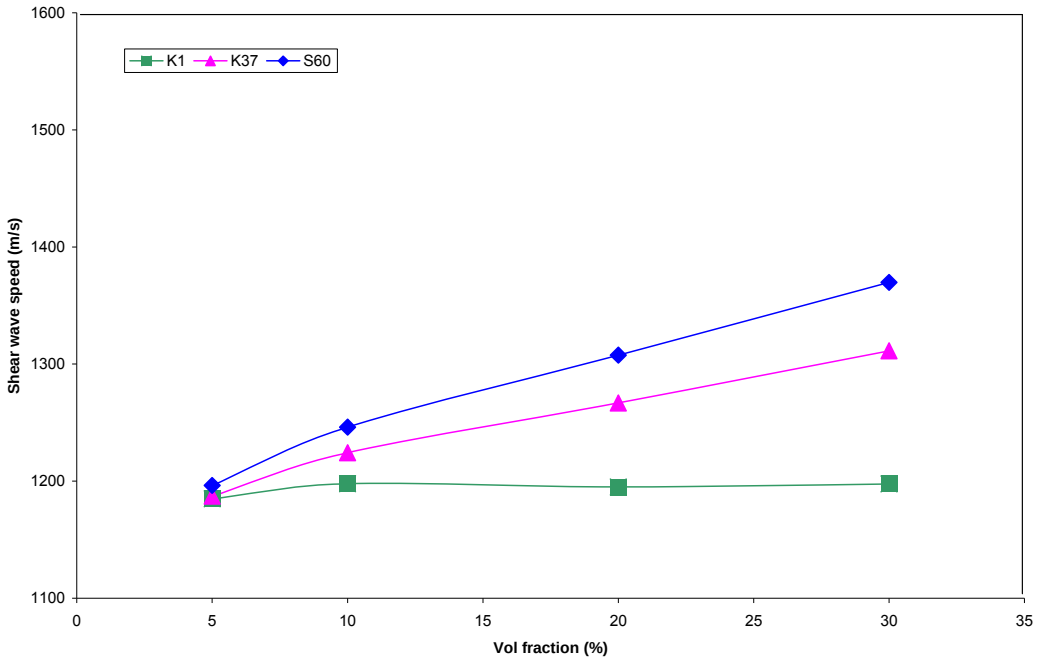

Figure 22. Shear Wave Speed of Syntactic Foams

Various material properties of syntactic foams could be obtained by measurement of ultrasonic wave speed in a material. For the given frequency of 1 MHz for longitudinal and 2.25 MHz for shear wave transducers, Poisson ratio, Young's modulus and shear modulus are calculated as shown in Table 7 [2]. Poisson's ratio decreased with increasing volume fraction as the material became less ductile

with increasing volume fractions. Values of Young's modulus and shear modulus showed similar trends to wave speed measurements.

Table 7. Elastic properties of Syntactic Foams

Volume Fraction of Sample, %	Longitudinal wave speed (m/s)	Shear wave speed (m/s)	Poisson Ratio	Density (kg/m^3)	E (Mpa)	G (Mpa)
Epoxy	2526	1179	0.361	1147	4337	1593
S60 - 5%	2579	1196	0.363	1092	4262	1563
S60 - 10%	2602	1246	0.351	1096	4600	1702
S60 - 20%	2689	1308	0.345	1032	4745	1764
S60 - 30%	2754	1370	0.336	975	4889	1830
K37 - 5%	2552	1187	0.362	1082	4152	1524
K37 - 10%	2576	1224	0.354	1063	4315	1593
K37 - 20%	2574	1267	0.340	984	4233	1579
K37 - 30%	2637	1311	0.336	897	4120	1542
K1 - 5%	2525	1185	0.359	1072	4090	1505
K1 - 10%	2485	1198	0.349	1032	3995	1481
K1 - 20%	2402	1195	0.336	940	3586	1343
K1 - 30%	2337	1198	0.322	844	3199	1210

Comparison of attenuation calculated from model of Mylavarapu and Woldesenbet and attenuation calculated experimentally here are shown in Figure 23. The theoretical model all increased with increasing volume fraction as attenuation due to absorption and scattering of microballoons were added to the attenuation of pure epoxy. Energy lost due to absorption of the epoxy matrix also plays an important part in both experimental and model analysis as most of the attenuation by absorption occurs in epoxy matrix. The model of Mylavarapu and Woldesenbet under-predicted the case for K1 size sphere and over predicted for the case of S60 and K37. The model under predicts due to the neglect of additional factors such as interaction of wave between particles. Over-prediction by the model for S60 and K37 is due to the assumption that the wave interacts with the microballoons, whereas the opposite occurs, the wave travels through the microballoons due to larger wavelength to

particle ratio and higher speed than epoxy matrix. There is also a variation due to the assumption that the 'planar wave' of the ultrasonic beam propagates and comes back through the specimen of thickness 'l' without alteration [5].

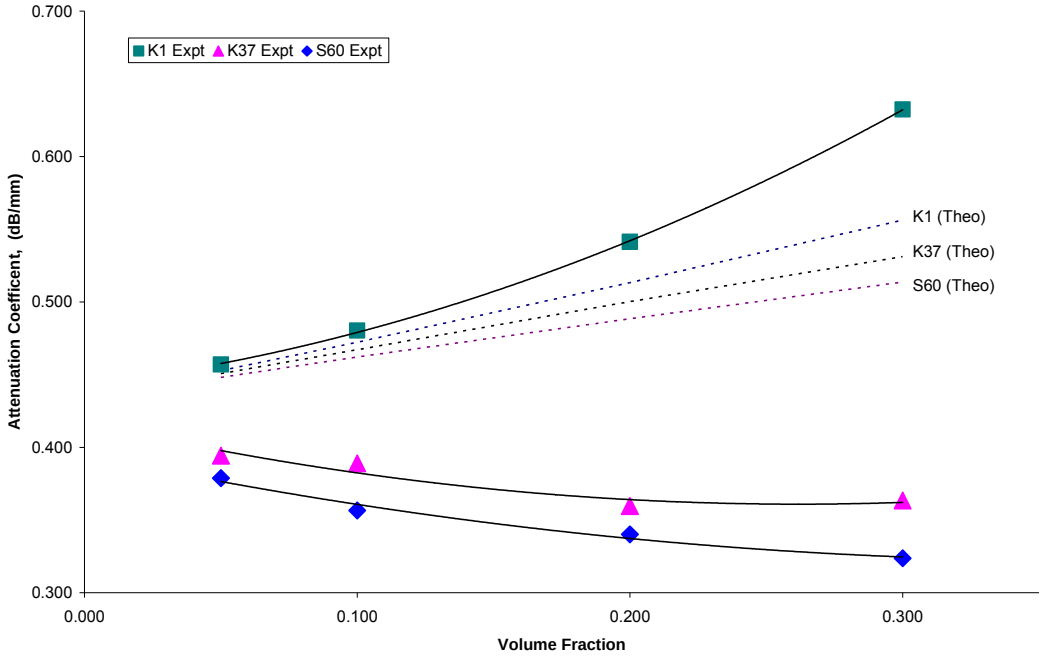

Figure 23. Comparison of Experimental and Theoretical Attenuation (Mylavarapu and Woldesenbet)

4.1.2 Ultrasonic Characterization of Graded Materials

Graded specimens as shown in Figure 24 were tested with ultrasonic immersion pulse echo testing. The specimen was 1.4 x 1.4 x 0.8 inches (35.6 x 35.6 x 20.3 mm). The layers were 0.2" (5.1 mm) thick. Five specimens of each type of syntactic foams were tested. Due to layering and the impedance mismatch between the layers, the analysis was more complicated and only the first front and back reflections from the end surface were used for calculating the attenuation coefficient and wave

speeds. Specimens were made with different number of layers and thicknesses and the best model was chosen based on clearly observable back reflections while maintaining a distinct gradation profile.

Figure 25 shows the reflected back longitudinal waves from each layer of S60 0-30 4FGM. Intermediate wave reflections off the intermediate layers were omitted for analysis. Also measurements were made from both sides of the syntactic foams i.e. the stiffer 30% volume fraction side and the epoxy side (0%). Both methods showed similar results in overall attenuation hence an average of the 10 readings was taken for each sample.

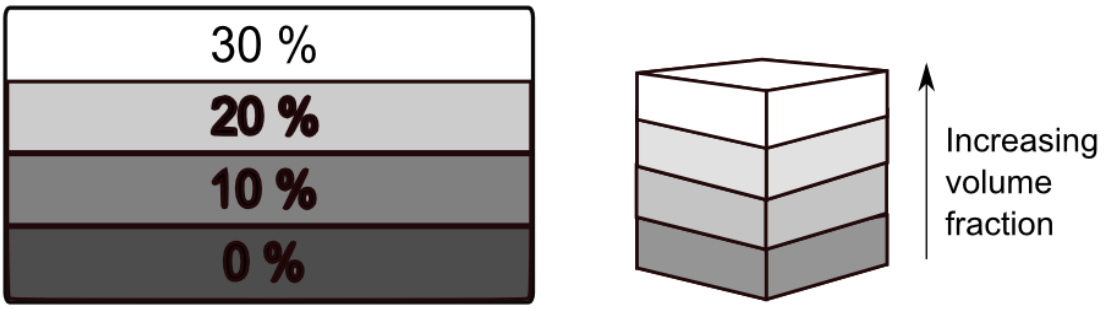

Figure 24. Pictorial representation of FGMs for Ultrasonic Testing

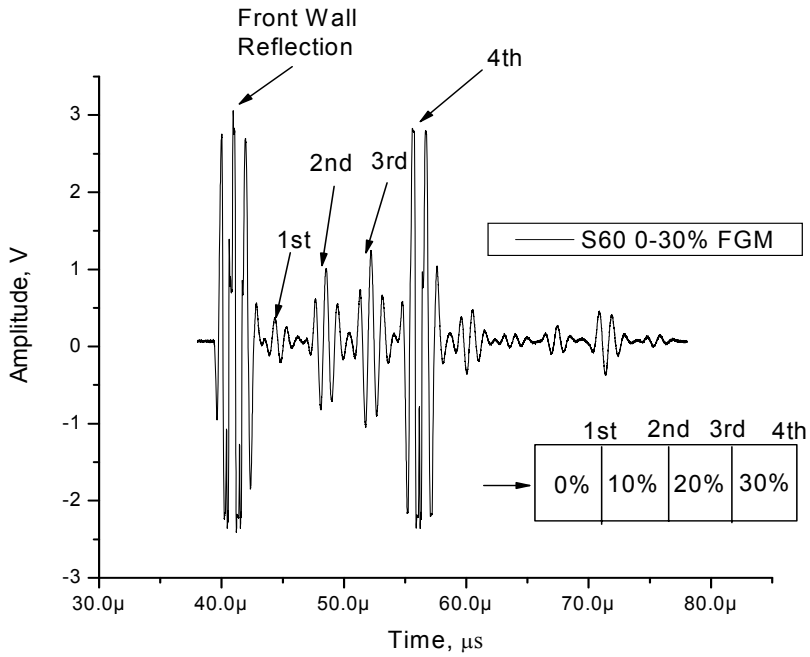

Figure 25. Amplitude vs. Time of S60-030-4FGM specimen with back wall reflections at from epoxy side

Longitudinal and shear wave values were calculated as shown in Figure 26 and 27. S60 FGM material showed the highest wave speeds. Shear wave speeds were about half the values of longitudinal wave speeds. The values obtained for wave speeds could not be directly related to the wave speeds values obtained for syntactic foams since different wave speed measurement techniques were used. Due to the multiple reflections at the layer boundaries, analysis of the energy loss occurred at each interface was ambiguous. Nevertheless, overall attenuation for the three different microballoon type FGMs foams could be compared with each other and similar trends to the non-graded syntactic foams were obtained as seen in Figure 28. Graded syntactic foams with overall attenuation are presented in Table 8. The attenuation for FGMs were calculated from the front wall reflection and the 4th back reflection as

shown in Figure 25. It can also be seen that the K1 FGMs had the highest attenution among the FGMs.

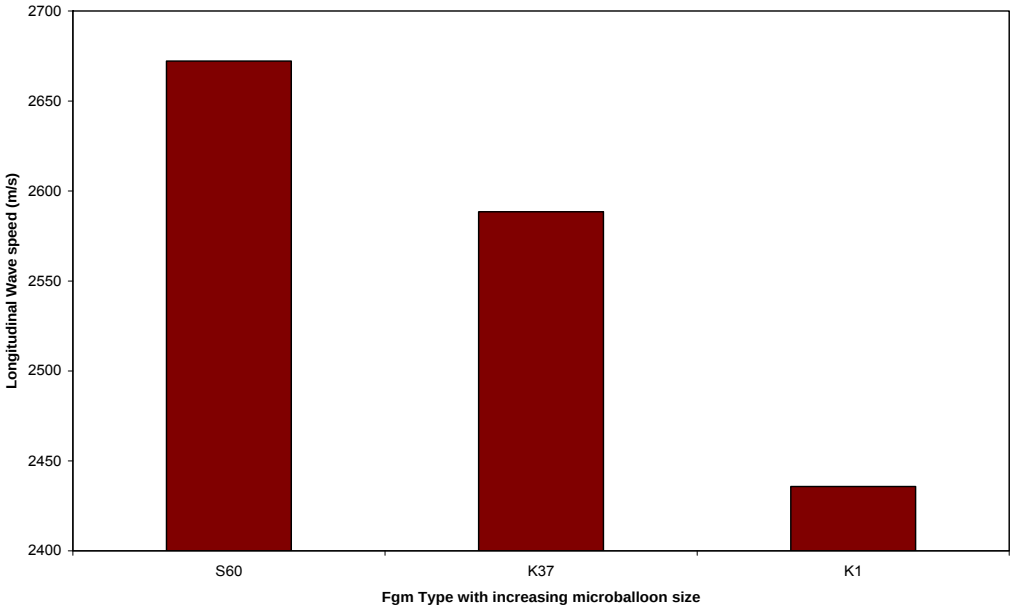

Figure 26. Longitudinal Wave Speed of FGM (0-30%) Foams

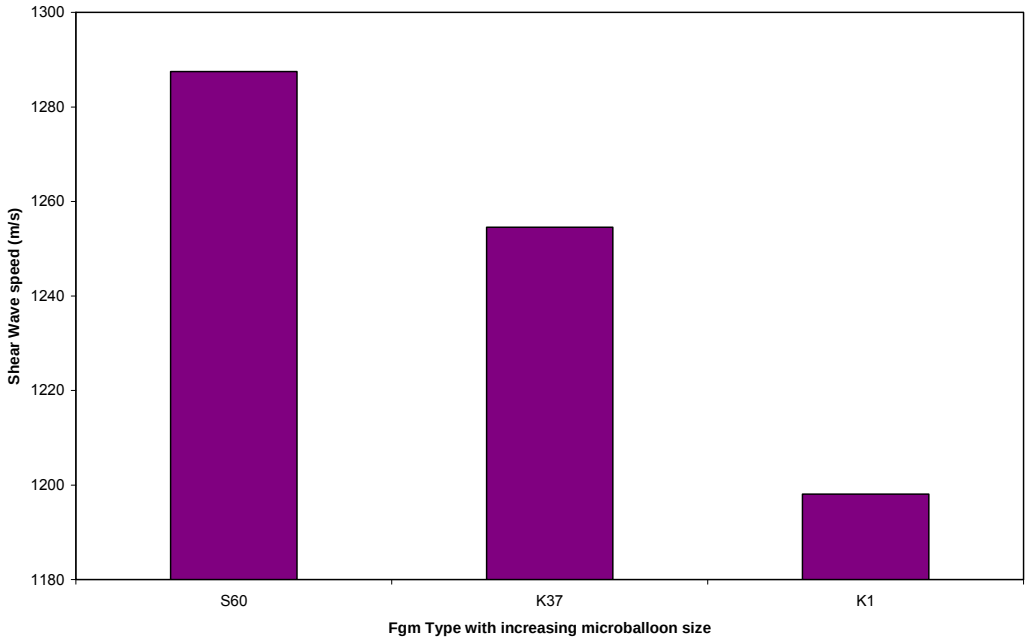

Figure 27. Shear Wave Speed of FGM (0-30%) Foams

Attenuation for FGM specimens

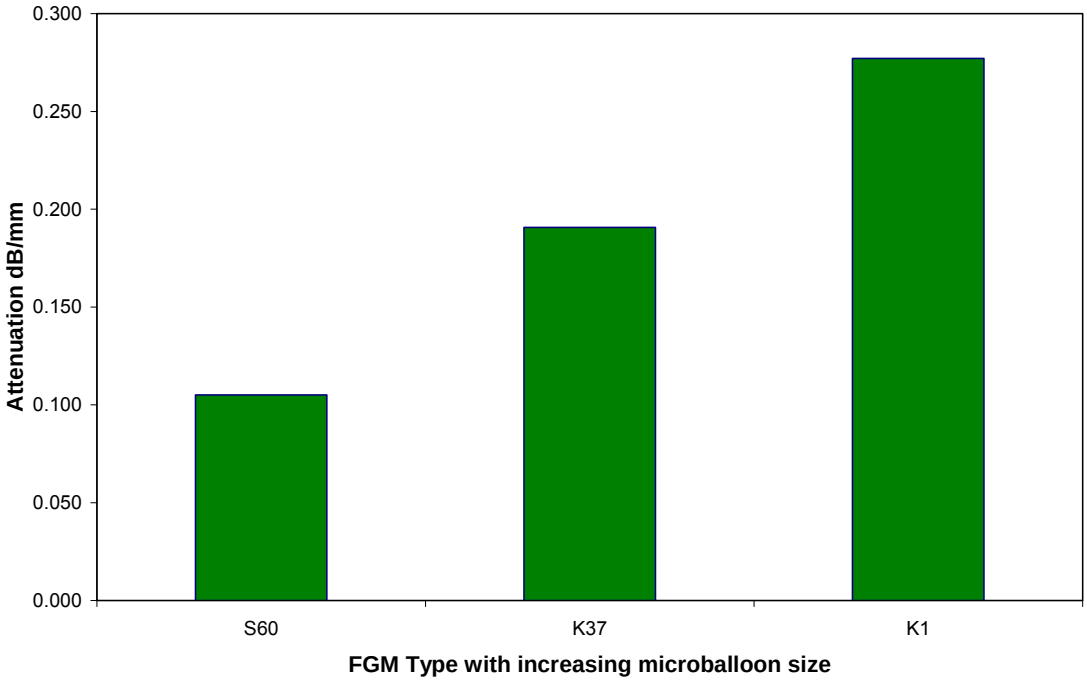

Figure 28. Attenuation of FGM (0-30%) Foams (front and 1st back reflection taken)

Table 8. FGMs ultrasonic properties

Sample FGM Type	Longitudinal wave speed (m/s)	Shear wave speed (m/s)	Attenuation from front and 1st back reflection (dB/mm)	Density (kg/m^3)
S60	2672 ± 2.72	1287 ± 1.02	0.105 ± 0.008	1066
K37	2588 ± 4.51	1255 ± 1.40	0.191 ± 0.015	1017
K1	2436 ± 4.51	1198 ± 0.62	0.277 ± 0.027	997

4.2 Compression Testing

The specimen size was 15.24 mm in thickness and 7.62 mm in diameter for the syntactic foams. The specimen size was 12.7 x 12.7 x 25.4 mm for FGM 0-40%

specimens. Six samples each were tested for both syntactic foams and FGM specimens. Typical stress strain features of the syntactic foams are shown in Figures 29-31. A comparison of stress strain curve of syntactic foam with plain epoxy resin is also shown in Figures 29-31.

4.2.1 Syntactic Foams

The compressive modulus is measured by the slope of the initial linear portion of the stress strain curve. The compressive strength is the first peak in the stress strain curve. It is similar to the curves obtained by [8]. The linear portion is up to the elastic limit after which plastic deformation occurs. After reaching the peak stress the stress drops and nearly becomes constant. This region is called the plateau region or densification region. In this stage the microballoons are crushed and the open space is occupied by the debris are matrix material while getting compressed [8]. Cracks start to appear at the ultimate compressive strength value. For our analysis, only the linear portion up to the peak stress was studied.

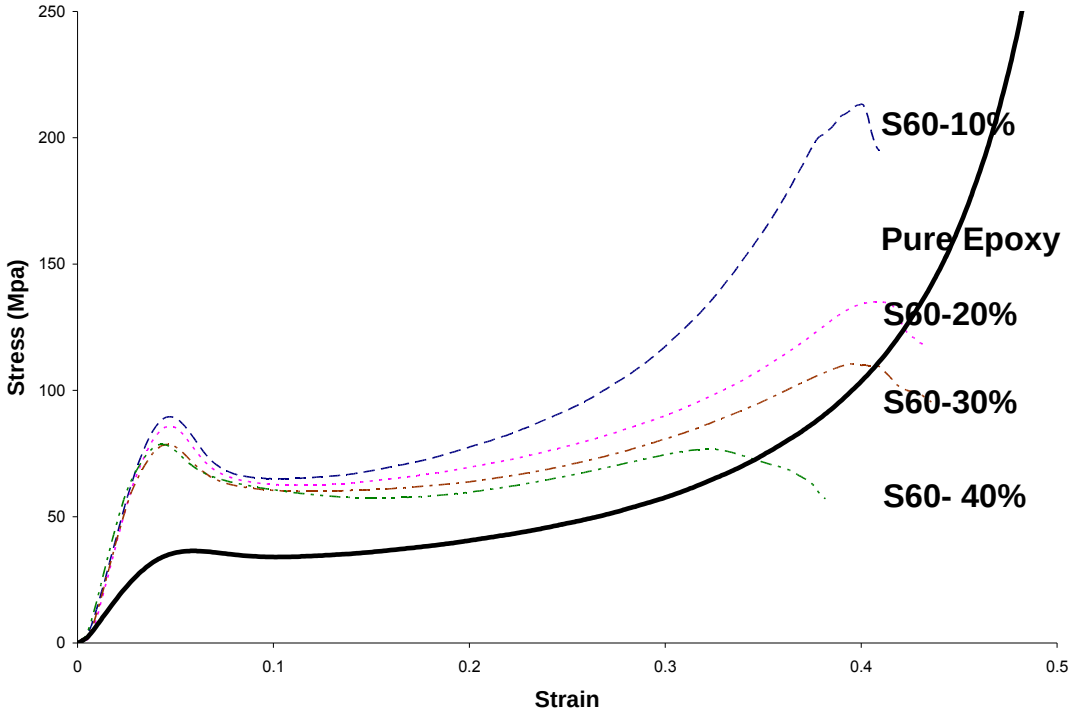

Figure 29. A typical stress-strain plot of S60 Syntactic foams including plain epoxy with different volume fractions

The compressive modulis and compressive yield stresses are shown for all syntactic foams in Table 9. The S60 syntactic foam had the highest value of compressive modulus and compressive yield strength for all type of syntactic foams followed by K37 type and then K1 type microballoons. It is observed that the syntactic foams have a wide range of modulus and strength values and can be tailored to a specific task if by manipulating to a certain volume fraction. Strain at peak stress (yield strength) is equivalent to the 0.048 strain for K37, 0.047 for S60, and 0.04 for K1 type syntactic foams.

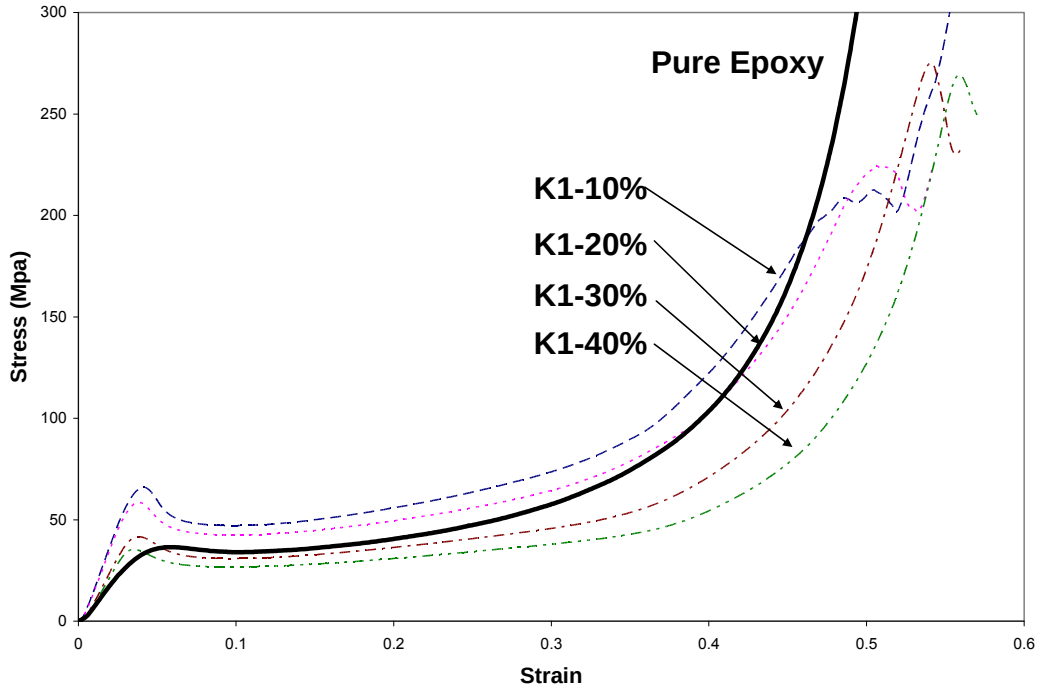

Figure 30. Stress-strain curves of K1 Syntactic foams including plain epoxy with different volume fractions

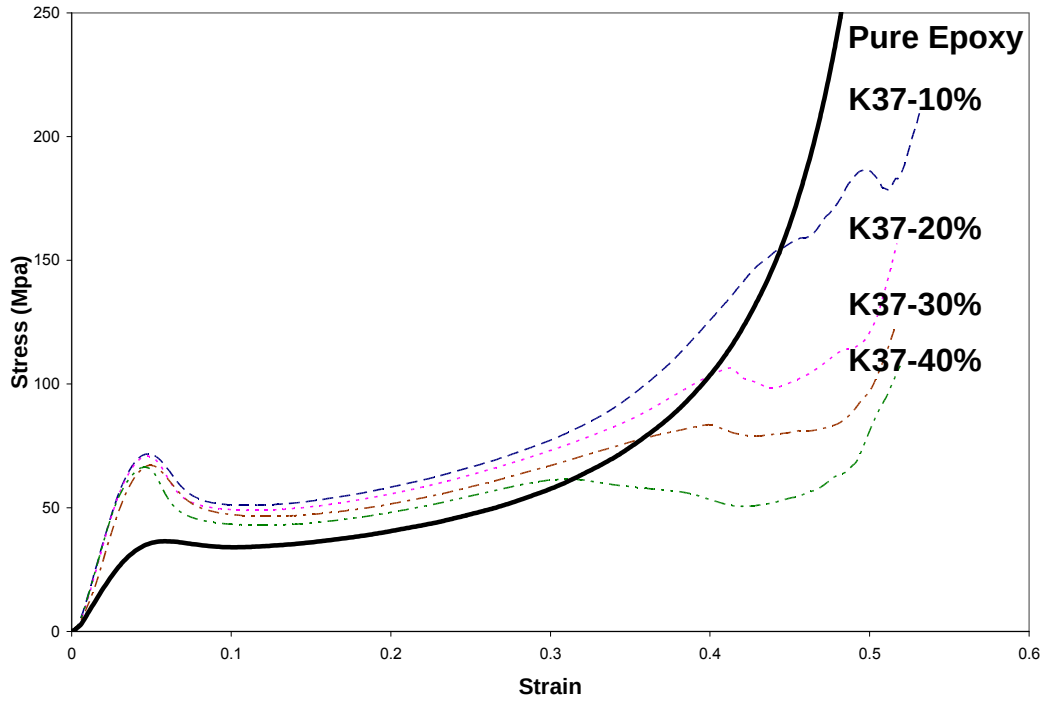

Figure 31. Stress-strain curves of K37 Syntactic foams including plain epoxy with different volume fractions

Table 9. Compressive Modulus and Yield Strength of Syntactic Foams

Type	Volume Percentage	Compressive Modulus (E) (Mpa)	Yield Strength (Mpa)
Epoxy	-	1038	36
K1	10%	2133	66
	20%	2034	59
	30%	1487	42
	40%	1325	35
K37	10%	2211	72
	20%	2265	71
	30%	2086	67
	40%	2242	66
S60	10%	2842	90
	20%	2881	86
	30%	2821	79
	40%	2984	79

Fracture accompanied by cracks formation along the direction of load was seen as shown in Figure 32. It can be seen that fewer cracks were formed for the 10% volume fraction than 40% volume fractions. Also there was more barreling effect seen for the lower volume fraction foams as the load was applied. This can be attributed by greater bonding and interfacial strength between the epoxy and microballoons at lower volume fractions.

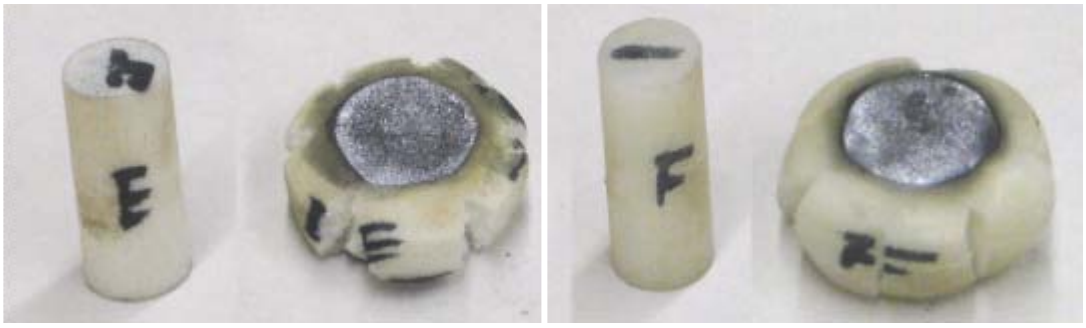

Figure 32. Cracks formation on K1-40 (left) and K1-10 (right) type syntactic foams

Further absorption energy (toughness) was calculated for each type of syntactic foams by calculating the area under the stress strain curve. Absorption energy curves

for all types of syntactic foams tested are shown in Figure 33. Absorption was calculated until the second peak stress in the stress strain graphs for all the materials. It can be seen that with the increase of volume fraction the material loses its toughness for all syntactic foams. The highest absorption was for the K1 type syntactic foam and the lowest for the S60 type syntactic foams. The decrease in absorption with increasing volume fraction is due to material becoming more brittle with the addition of microballoons hence decreasing the strain at which fracture occurs. Also, the values of ultimate strength decreased for the S60 and K37 type foam whereas it increased for K1 type foam as shown in Figures 29-31. The increase in ultimate strength for the K1 type foam is due to larger voids created when microballoons fractured. It takes longer compression time required to fill up void with the debris of fractured microballoons. The strain at ultimate strength is higher for K1 type microballoons than the other microballoons type examined. The absorption value of pure epoxy was 55 Mpa–mm/mm.

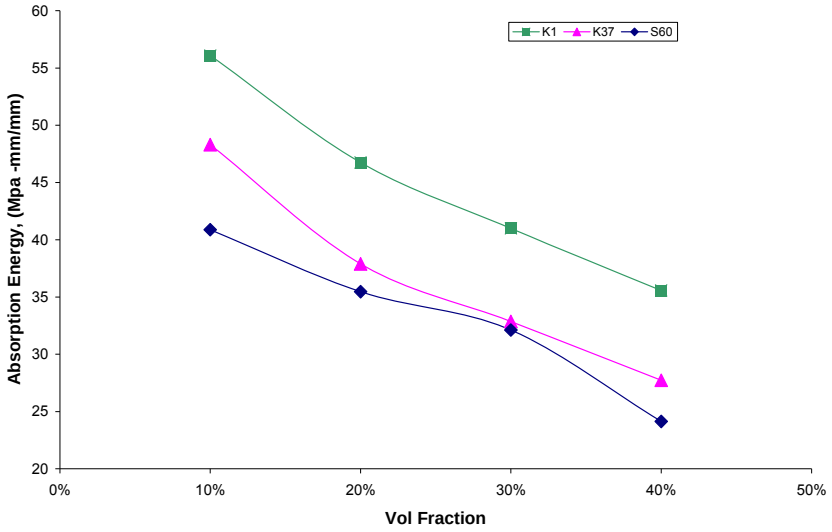

Figure 33. Absorption Energy of Syntactic foams during Quasi-static compression testing

4.2.2 Functionally Graded Materials

Functionally graded syntactic foams with increasing volume fractions with the orientation were manufactured as shown in Figure 34. The volume fraction range was 0-40% with five layers of gradation. Each layer was 0.2” (5.1 mm) thick. The color of the layers turns from transparent green to opaque white with the addition of layers.

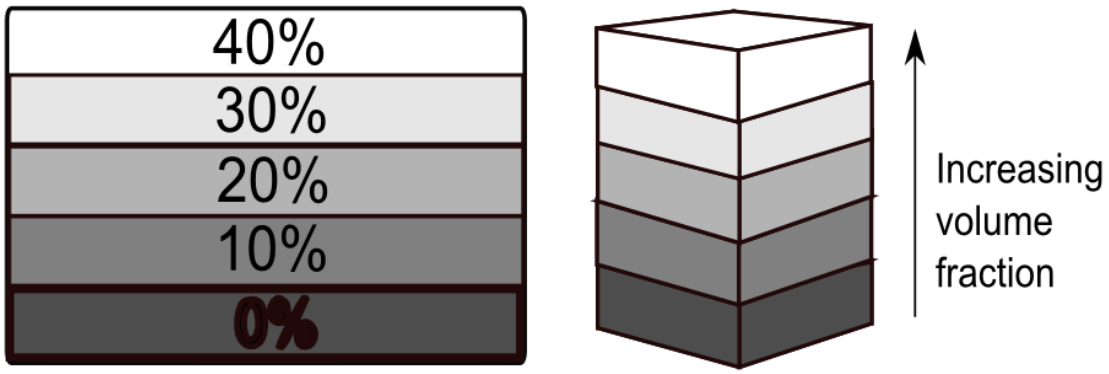

Figure 34. FGM 0-40% specimens for compression testing

The stress strain curves for the FGM specimens are shown in Figure 35. The curves represent an average of 6 samples for each microballoon type. Curves similar to those of the syntactic foams are observed for the graded specimens with S60 having the highest yield strength and modulus from all the 3 foams, as shown in Table 10. Compressive modulus and yield values are between the ranges obtained for syntactic foams of 0-40%.

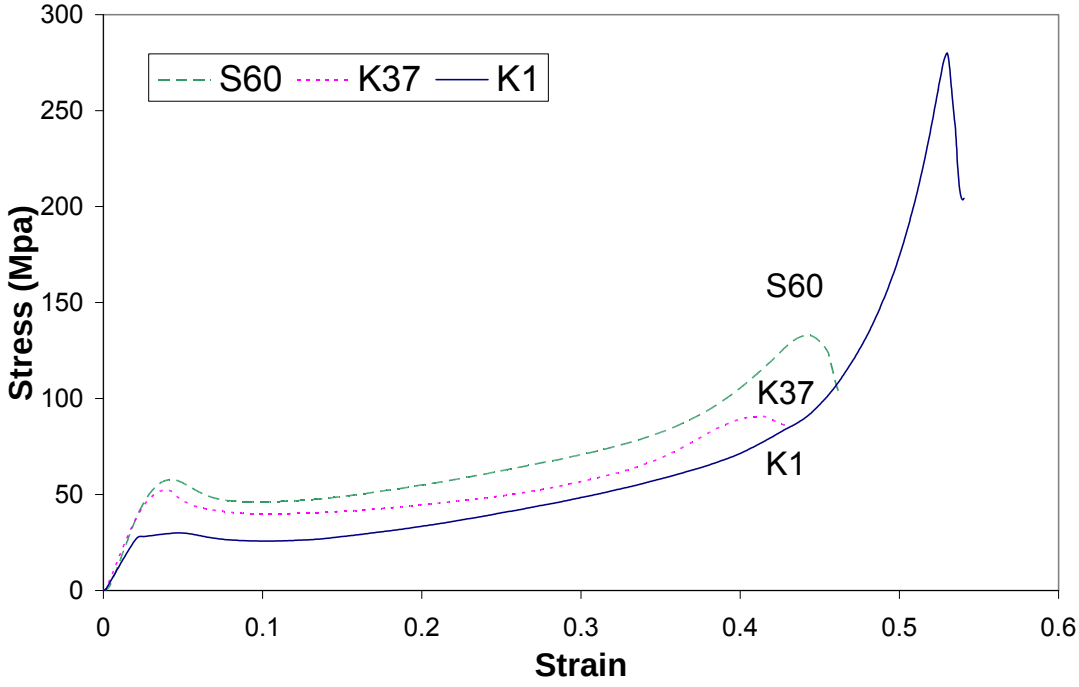

Figure 35. Stress Strain Curves for FGMs 0-40% syntactic foams

Table 10. Compressive Modulus and Yield Strength of FGMs

Sample	E (Mpa)	Ys(Mpa)	Energy Absorption (Mpa-mm/mm)
S60	2150	60	31
K37	1962	52	23
K1	1430	28	35

Figure 36, shows a sample of K37-040-5FGM after compression testing. Barreling effect was seen in all specimens and cracks initiated at the stiffer side i.e. the 40% side of the specimens. The cracks ran along the middle of the specimen edge in the vertical direction parallel to the applied load.

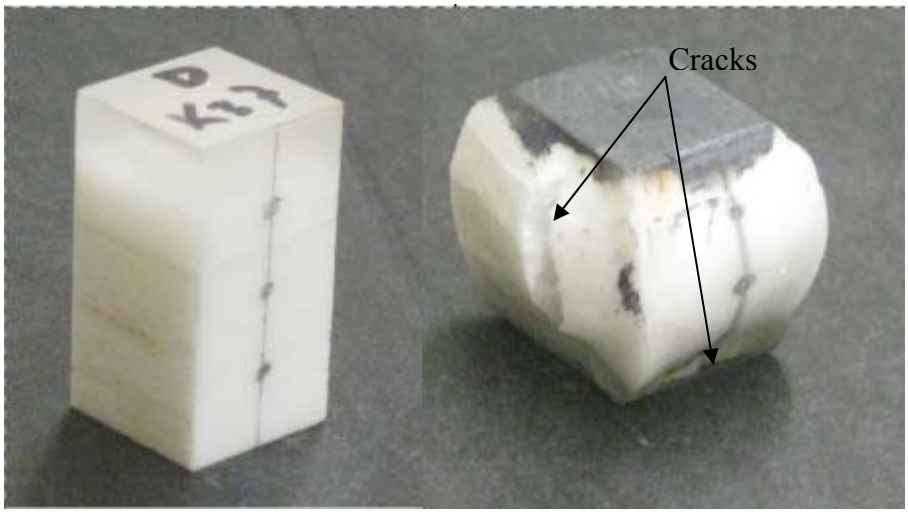

Figure 36. Graded K37 specimen with cracks after compression testing

Values of compressive modulus and yield strength all were lower than the syntactic foam values for similar densities. This is attributed to the weaker interfacial bonds between layers compared to the more uniform bond in syntactic foams between particulates and epoxy. The absorption of FGM specimens were calculated from the stress strain curves. Figure 37 shows the absorption of FGM specimens. K1 type FGM specimens showed the highest energy absorption due to the high ultimate strength value reached during densification of the microballoons. Strain at failure was 0.044 for S60, 0.041 for K37, and 0.053 for K1 type syntactic foams. A decrease in 6% for S60 and 15% for K37 type FGM was calculated in comparison with plain syntactic foams for strain at failure. Strain at failure increased by 33% for the K1 type FGM specimens. This increase is attributed to the high energy absorption of K1 type syntactic foams and layer contribution to the densification of microballoons.

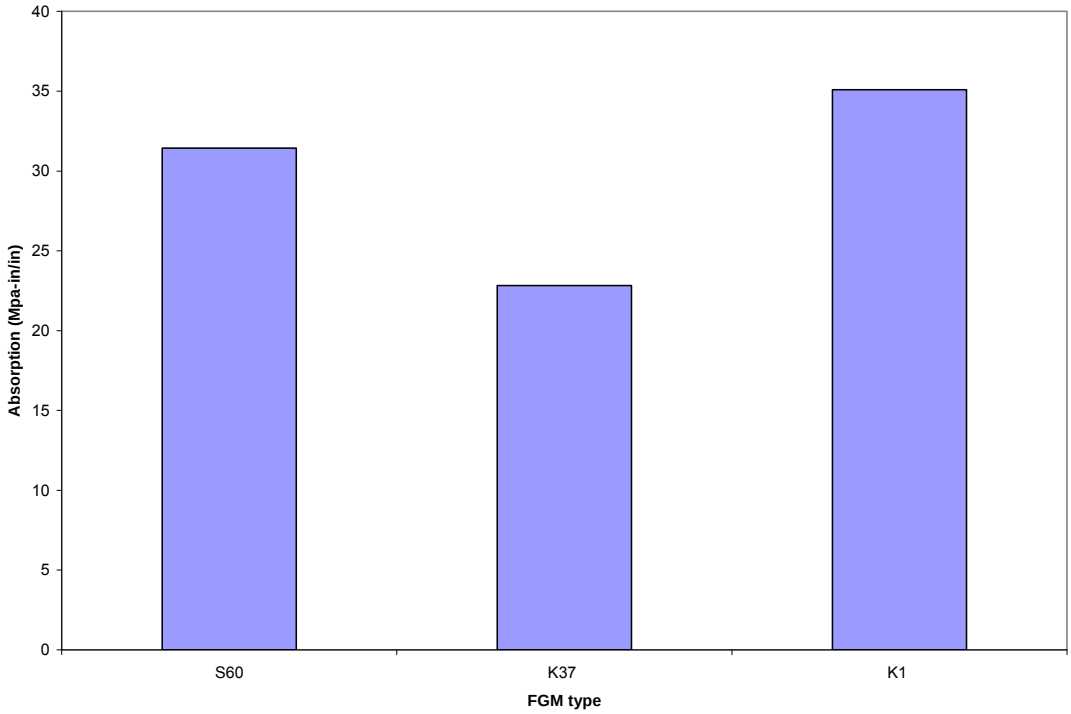

Figure 37. Absorption Energy for FGMs 0-40% syntactic foams

4.3 Low Velocity Impacts

Low velocity impacts are the most common type of impacts experienced by materials. Collision occurring during parking, or dropping of a hammer are examples of such instances. During the events a small indentation may mark the outside while significant damage occurs internally. This could cause the load bearing capacity of a structure to reduce significantly and failure to occur soon afterwards. Hence low velocity impacts must be studied for these syntactic foams.

Six samples of syntactic foams and FGM (0-40%) 5 layered specimens were tested during this study. The load/energy vs. the time was recorded for the contact loading time as shown in Figure 38. It shows the load that is exerted on the sample while the tup assembly is in contact with the specimen during impact. The energy

corresponding to the maximum load during impact is known as initiation energy. It is the energy that is absorbed by the material before failure. It can also be defined as the strain energy transferred elastically by the target [9]. The propagation energy is defined as the difference between the Maximum Energy and the Initiation energy. It includes all the energy absorption of the specimen during failure. Crushing of microballoons and crack formation are all accounted for in Propagation Energy. An ideal system for highest energy absorption prior to failure would consist of high Initiation Energy but absorption after failure to have high Propagation energy. Impact velocity of 3m/s was chosen for analysis for all tests. The dip in the energy curve after reaching maximum energy is due to impactor being pushed back by the specimen after reaching maximum deflection. Due to force acting in the negative direction, the impact force does negative work on the specimen and a portion of strain energy is transferred back to the impactor hence a decline in total energy.

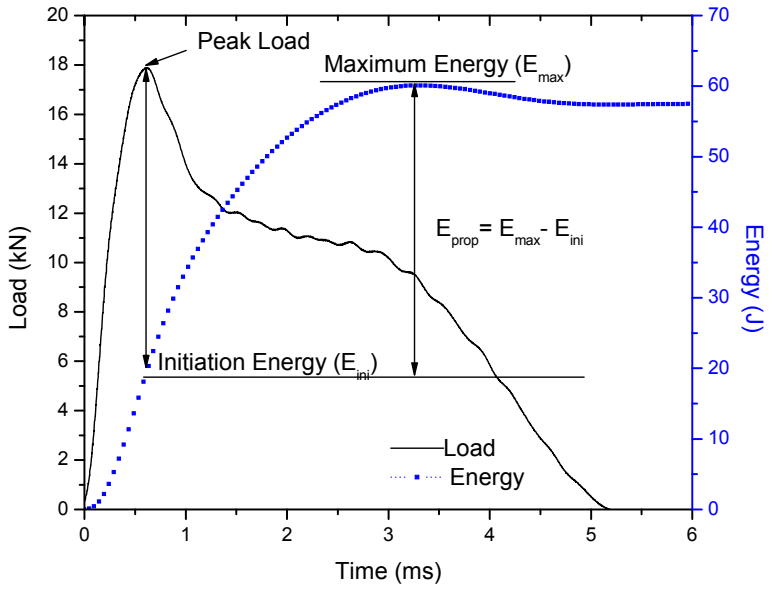

Figure 38. Load/Energy vs. Time of low velocity impacts

4.3.1 Syntactic Foams Low Velocity Impacts

The specimen size was 11.43 mm in diameter and 22.86 mm in height. Figure 39 shows the maximum peak load obtained for all types of syntactic foams. The value is an average of six samples tested for each specimen. It can be clearly seen that the peak load decreases for all type of syntactic foams with increasing volume fraction. It is due to the increase in voids in the material causing the material to weaken. S60 type syntactic foams showed the highest peak load values of all the other type of microballoons. The peak load values follow the trend of smallest size microballoon with highest crush strength having higher load bearing properties similar to quasi static compression testing.

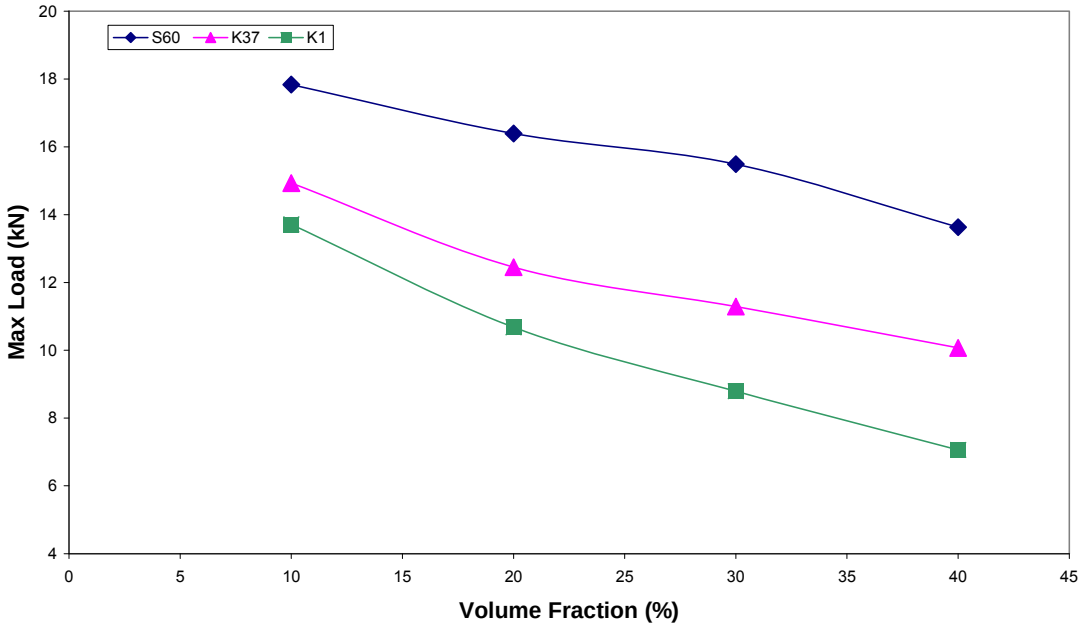

Figure 39. Maximum load of syntactic foams at 3m/s Impact

Table 11 can be used to further analyze the absorptive behavior, where initiation and propagation energy are obtained for each type of syntactic foam according to volume fraction. Numerical values for the peak load are also given in Table 11. The highest initiation energy was obtained for pure epoxy which also has the highest peak load, suggesting pure epoxy has higher load bearing capacity at higher strain rates. It can be seen that with increasing volume fractions initiation energy decreased, and that propagation energy increased for all type of syntactic foams. This denotes that the strength of the syntactic foams decreased with the addition of microballoons and better absorption during propagation was seen.

Table 11. Impact testing of Syntactic Foams at 3m/s

Type	Volume Fraction	Velocity (m/s)	Initiation Energy (J)	Propagation Energy (J)	Peak Load (kN)
Epoxy	0	3	19.08	41.42	17.85
S60-10	10	3	18.49	41.55	17.84
S60-20	20	3	14.33	45.63	16.39
S60-30	30	3	11.28	48.77	15.49
S60-40	40	3	7.34	52.69	13.63
K37-10	10	3	13.44	46.53	14.93
K37-20	20	3	9.56	50.42	12.45
K37-30	30	3	6.26	53.71	11.29
K37-40	40	3	6.26	53.74	10.07
K1-10	10	3	12.27	47.73	13.71
K1-20	20	3	9.68	50.33	10.68
K1-30	30	3	8.30	51.73	8.80
K1-40	40	3	3.17	56.88	7.06

The highest propagation energy was seen for the K1 type syntactic foams due to the larger microballoon size and ease of fracture than the other two microballoons.

Figure 40 shows an impacted specimen of S60-10 type syntactic foams. It can be seen that there are multiple cracks which have been propagated cracks along the length of specimen. On the other hand, a higher volume fraction specimen such as K1- 40 type syntactic foams was crushed as seen in Figure 41.

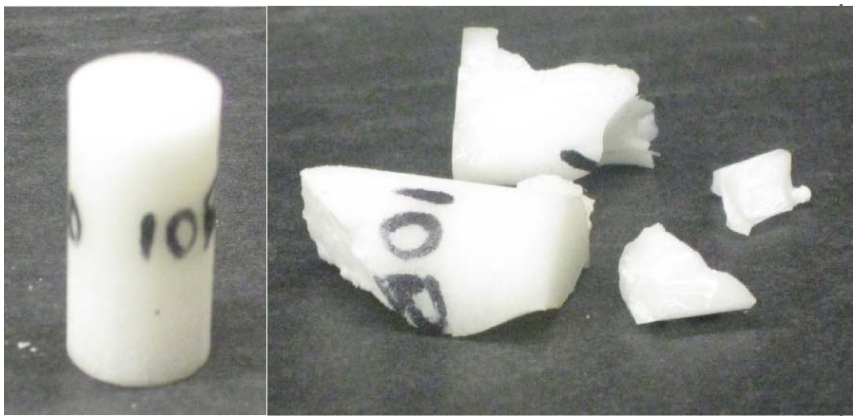

Figure 40. Impacted specimen of S60-10 syntactic foam

Figure 41. Impacted specimen of K1-40 syntactic foam

4.3.2 Funtionally Graded Materials Low Velocity Impacts

Graded specimens of 0-40% FGMs were also tested. The specimen size was 12.7 x 12.7 x 25.4 mm. Initiation and propagation energy of the specimens can be

seen from Figure 42. The propagation energy are higher and initiation energy smaller for increasing bubble size of FGMs. This trend is similar to plain syntactic foams. Lower density layers in the FGMs tend to absorb more energy during failure whereas the higher density layers add strength to the material. It can be seen that the S60 type FGMs showed a higher peak load than the other two FGMs as shown in Figure 43. S60 FGMs showed higher load bearing capacity for impact loading than plain syntactic foams with similar density as shown in Table 12.

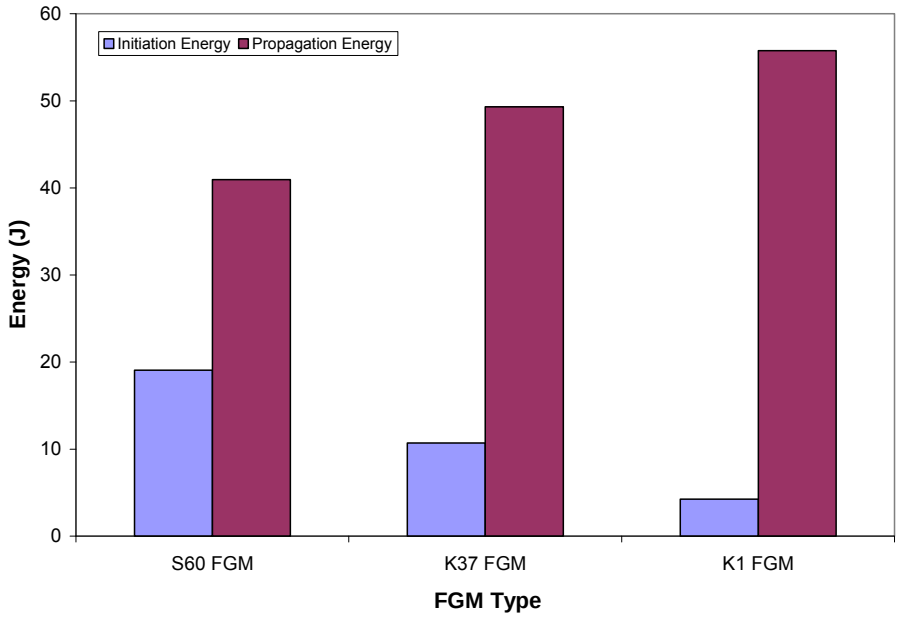

Figure 42. Initiation and Propagation Energy of FGMs

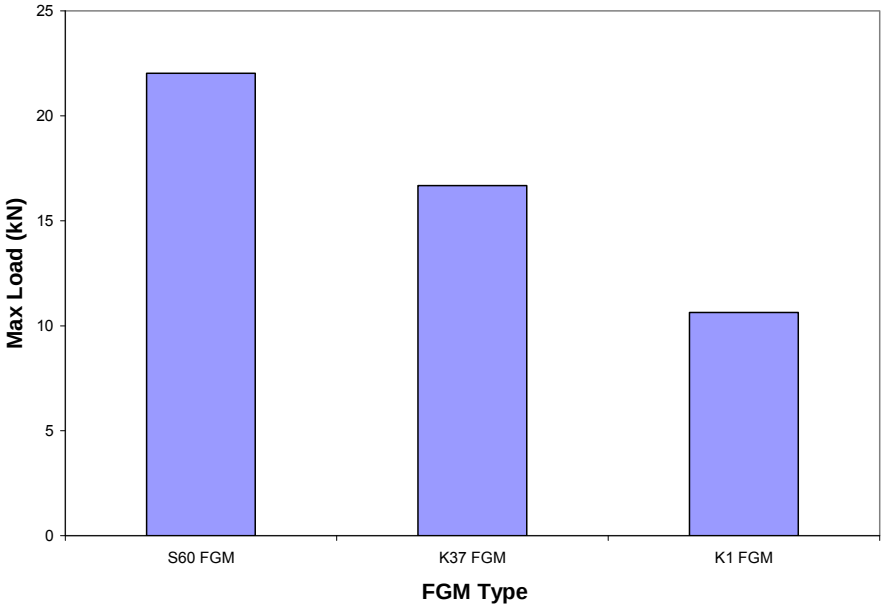

Figure 43. Maximum (peak) load of FGMs during Impact at 3m/s

Table 12. Comparison of FGMs peak load with plain syntactic foams

Type	Density (kg/m^3)	Peak load (kN)
S60-040-5FGM	1064	22
K37-10	1063	15
S60-10	1096	18
S60-20	1032	16

Figure 44 and 45 show the impacted specimens of FGMs. It can bee that failure of S60-040-5FGM are due to crack propagation whereas for K1-040-5FGM the failure is due to total crushing of the microballoons. Also S60-040-5FGM is stiffer than the K1-040-5FGM and hence K1-040-5FGM has higher propagation energy than S60-040-5FGM.

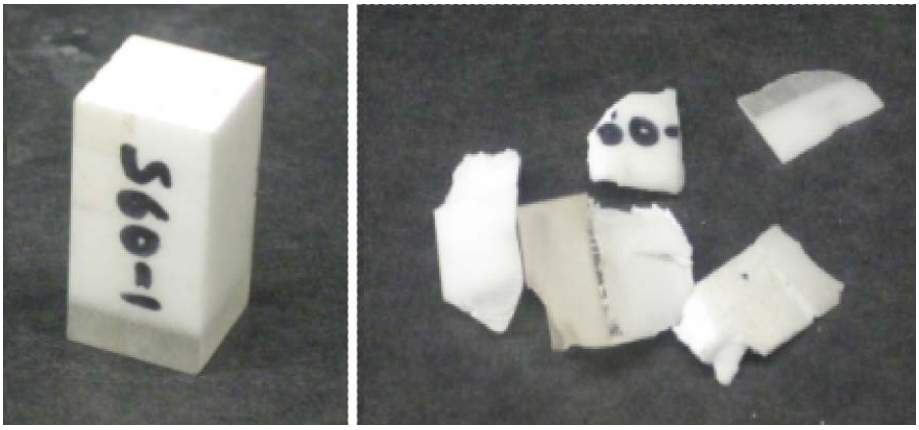

Figure 44. Impacted specimen of S60-040-5FGM

Figure 45. Impacted specimen of K1-040-5FGM

References:

1. R. Truell, C. Elbaum, and B. Chick, *Ultrasonic Method in Solid State Physics* (Academic, New York, 1969).

2. www.olympus-ims.com, Olympus Transducer Catalog, (2009), Retrieved August 11, 2009, from http://www.olympus-ims.com/data/File/panametrics/panametrics-UT.en.pdf

3. www.ndt-ed.org, Reflection and Transmission Coefficients (Pressure), (2001). Retrieved March 4, 2009, from http://www.ndt-ed.org/EducationResources/CommunityCollege/Ultrasonics/Physics/reflectiontransmission.htm

4. ASTM E664 –93 (2005) Standard Practice for Measurement of the Apparent Attenuation of Longitudinal Ultrasonic Waves by Immersion Method, ASTM International, West Conshohocken, PA, USA

5. Phani Mylavarapu, Eyassu Woldesenbet, A predictive model for ultrasonic attenuation coefficient in particulate composites, Composites Part B: Engineering, Volume 41, Issue 1, January 2010, Pages 42-47, ISSN 1359-8368

6. P. Mylavarapu and E. Woldesenbet, ―Characterization of syntactic foams- an Ultrasonic Approach, Journal of Cellular Plastics, Vol. 44, No. 3, 203-222, 2008.

7. S. Biwa, S. Idekoba, N. Ohno, Wave attenuation in particulate polymer composites: independent scattering/absorption analysis and comparison to measurements, Mechanics of Materials, Volume 34, Issue 10, October 2002, Pages 671-682

8. Nikhil Gupta, Eyassu Woldesenbet, Patrick Mensah, Compression properties of syntactic foams: effect of cenosphere radius ratio and specimen aspect ratio, Composites Part A: Applied Science and Manufacturing, Volume 35, Issue 1, January 2004, Pages 103-111

9. Guoqiang Li, Nji Jones, Development of rubberized syntactic foam, Composites Part A: Applied Science and Manufacturing, Volume 38, Issue 6, June 2007, Pages 1483-1492

CHAPTER 5

CONCLUSIONS AND RECOMMENDATIONS

Syntactic and FGMs materials were studied to bring to light the effects of volume fraction and size of microballoons on the wave interaction using ultrasonic techniques. Additional, quasi-static compression testing and low velocity impacts ests were conducted on these materials to understand their mechanical behavior at different strain rates.

5.1 Ultrasonic Testing

1. Longitudinal and Shear wave speeds were highest for the smallest microballoon size (S60) syntactic foams. Material wave speed increased with volume fraction up to 30%. Similar results were obtained with K37 type syntactic foams. However, for K1 syntactic foams, the wave speeds decreased with increasing volume fraction and were lower than that of virgin epoxy. This suggests that there is a certain particulate size for which at a particular frequency, the wavelength of the wave has more interactions with the microballoon. This claim is supported by the fact that wavelength to particle size ratio of S60 is smaller than that of the other types of syntactic foams tested. The range of wave speeds for all type of syntactic foams was from 2337-2754 m/s for the longitudinal and 1185-1370 m/s for the shear waves.
2. Young's modulus and Shear modulus were evaluated using the wave speed values obtained. It is applicable to consider the syntactic foam as a non dispersive media and obtain similar wave speed measurements from all sides

3. Attenuation values ranged from 0.324 to 0.632 dB/mm for all the syntactic foams tested. Attenuation was highest for the K1 type syntactic foams and increased with volume fraction. It suggests that scattering was a dominant factor in controlling the attenuation behaviors of these materials. Attenuation decreased with increasing volume fraction for S60 and K37 because of the increasing speed of the waves and the decreasing interaction with the microballoons. Absorption due to epoxy was also one of the main attenuation parameters. Clusters of particles for smaller size microballoons at higher volume fractions also affected the theoretical [1] and experimental values. Values of attenuation coefficient predicted by the theoretical model suggests more experimental results on different size microballoons must be obtained and that parameters such as cluster to cluster wave interaction, scattering due to particle to particle interaction, internal losses due to heat, friction must be taken into account in the overall model.

4. Ultrasonic tests on FGMs suggest higher degree of interaction due to the impedance mismatch between each layer. Overall attenuation calculated from the front and 1st back reflection of the last layer suggest similar trend as syntactic foams with K1 FGMs having higher attenuation than K37 and S60 syntactic foams. Wave speeds were also higher for the smaller size microballoons S60 FGMs than K37 and K1 FGMs.

5.2 Compression Tests

1. Increasing of compressive yield strength by lowering the volume fraction of microballoons and by using smaller size microballoons was seen for these tests on syntactic foams as supported by [2]. The values of compressive modulus and compressive yield ranged from 1325-2984 Mpa and 35-90 Mpa respectively. This suggests a wide load range capacity for these syntactic foams.
2. Failure was mainly due to crack propagation after the densification of the syntactic foams during compression. Cracks propagated in the direction of the load. Fewer cracks were observed for lower volume fractions than higher volume fractions. This is due to weaker particle to matrix bond strength since a higher number of microballoons are present with increasing volume fraction.
3. Values of compressive modulus and compressive yield strength were highest for S60 FGMs. This is due to the high crush strength of S60 microballoons. Barreling effect was seen on all FGMs during compression. Cracks started at

the high volume fraction side for all FGMs and ran in the direction of applied load.

4. Values of compressive modulus and yield strength all were lower than those of the syntactic foam for similar densities. This is attributed to the weaker interfacial bonds between layers compared to the more uniform bond in syntactic foams between the particulates and the matrix.

5.3 Low Velocity Impact Tests

1. Maximum peak load decreased with increasing volume fraction suggesting weaker strength at higher volume fractions similar to quasi static compression tests. Higher values peak loads were obtained for the S60 syntactic foams than for the others due to the higher crush strength [Table1] of these microballoons. The peak load was highest for Epoxy 17.85 kN and lowest for K1 40% at 7.06 kN.
2. For 60 J of energy input into each test, initiation energy and propagation energy were calculated for all syntactic foams. For all three different microballoon size syntactic foams Initiation energy decreased and Propagation energy increased suggesting absorption during failure was higher for the higher volume fraction foams. Addition of microballoons tended to absorb more energy after reaching the peak load which suggests the importance for the use microballoons in creating damage absorbent materials. Initiation energy decreased for higher volume fractions syntactic foams due to its weaker load bearing capacity at impact velocities of 3m/s.

3. Because of the variations in stiffness of these syntactic foams, higher volume fraction syntactic foams were crushed during loading whereas in lower volume fraction foams, fracture occured by crack propagation and shear failure.
4. Higher initiation energy was obtained for the S60 FGMs than for the other FGMs because these FGMs have higher strength and stiffness than those with other types of microballoons. Propagation energy was higher for the K1 type syntactic foams. Damage to larger size syntactic foams (K1) featured significant crushing, whereas post analysis of S60 (smallest size) type syntactic foam showed multiple crack propagation.
5. Peak load of S60 FGMs was higher than plain syntactic foam of similar density. This suggests that the gradation or intermediate layers distribute load throughout all the layers for better load bearing capacity during compression for a particular microballoon size. Peak load values decreased with the increase in size of the microballoons.

5.4 Recommendations

1. Expansion into solid particulate composites and their behavior to ultrasonic wave propagation would be beneficial in choosing materials for determining and comparing the results of their wave speed and attenuation to those of syntactic foams.
2. Better methods of gradation of microballoons could improve properties of FGMs and reduce the interlayer reflection occurring at each interface for evaluating attenuation coefficient.

3. The study does not incorporate attenuation by higher frequency transducers as there was a limitation with some of the settings of the pulser/receiver unit and the material being tested was highly attenuating.
4. Further attenuation behavior of acoustic wave related to stress wave attenuation could be studied using Split Hopkinson bars.
5. Impact tests at higher strain rates of $100s^{-1}$- 600 s^{-1} using the Split Hopkinson bar apparatus would be useful for determining yield or flow stress at higher impact velocities.
6. Design of newer composites by incorporatiing or adding of higher strength materials with different shapes and sizes of microballoons can help improve material properties and wave attenuation.

References:

1) P. Mylavarapu and E. Woldesenbet, ―Characterization of syntactic foams- an Ultrasonic Approach, Journal of Cellular Plastics, Vol. 44, No. 3, 203-222, 2008.

2) Nikhil Gupta, Eyassu Woldesenbet, Patrick Mensah, Compression properties of syntactic foams: effect of cenosphere radius ratio and specimen aspect ratio, Composites Part A: Applied Science and Manufacturing, Volume 35, Issue 1, January 2004, Pages 103-111

APPENDICES

Appendix A: Ultrasonic Samples

S60-5, S60-10, S60-20 and S60-30 samples

K37-5, K37-10, K37-20 and K37-30 samples

K1-5, K1-10, K1-20 and K1-30 samples

Syntactic Foams compared to Pure Epoxy sample

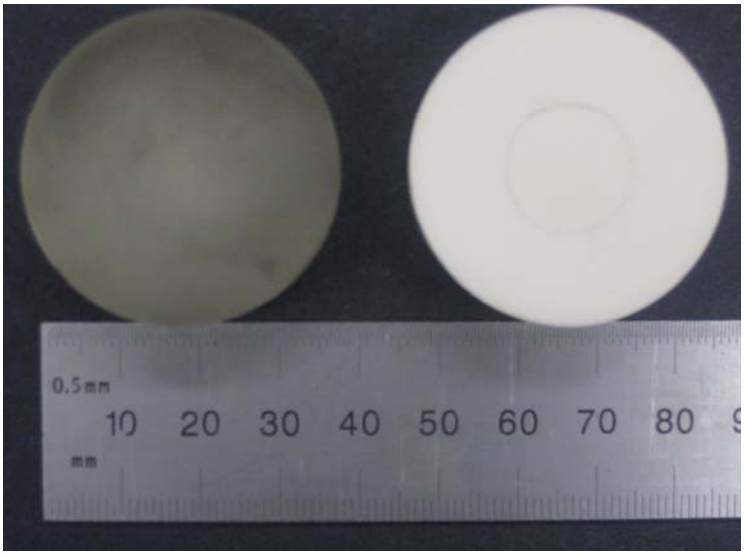

FGMS for Ultrasonic Testing

S60-030-4FGM, K37-030-4FGM and K1-030-4FGM

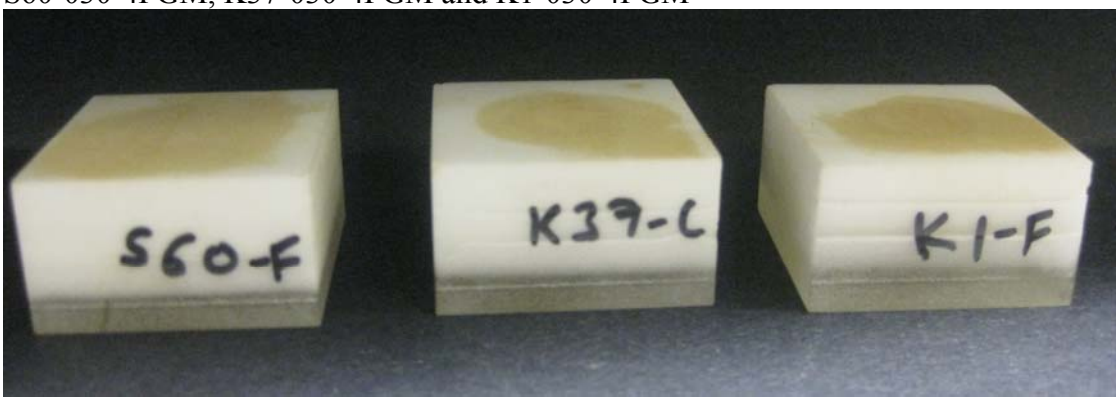

Size of FGM specimens for Ultrasonic Testing

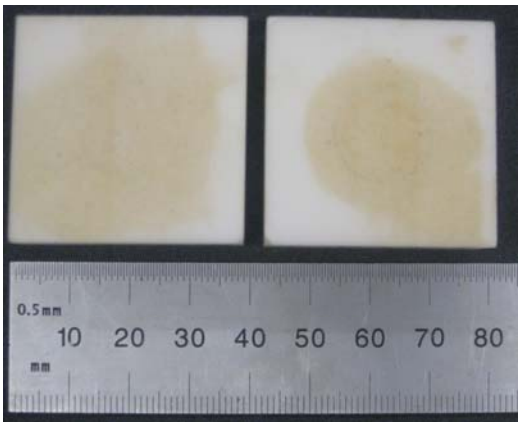

Appendix B: Ultrasonic Transducer Properties

For 1 MHz Immersion Transducer

OLYMPUS

Tel: 781-419-3900
www.olympusndt.com

TRANSDUCER DESCRIPTION

PART NO.: V303
SERIAL NO.: 676041
DESIGNATION: IMMERSION

FREQUENCY: 1.00 MHz
ELEMENT SIZE: .5 in. DIA.

TEST INSTRUMENTATION

PULSER/RECEIVER: PANAMETRICS 5052UA #1
DIGITAL OSCILLOSCOPE: LeCroy LT342 / SN: LT34202249
TEST PROGRAM: TP103-3 VER. 108C27
CABLE: RG-58 A/U LENGTH: 4FT

TEST CONDITIONS

PULSER SETTING: ENERGY: 1 ; DAMPING: 200 OHMS
RECEIVER SETTING: ATTN: 30dB ; GAIN: 40dB
TARGET: 2 in. SILICA
JOB CODE: TP200

WATER PATH: .987 in

MEASUREMENTS PER ASTM E1065

WAVEFORM DURATION:
-14DB LEVEL --- 2.300 US
-20DB LEVEL --- 2.840 US
-40DB LEVEL --- 4.720 US

SPECTRUM MEASURANDS:
CENTER FREQ. ------ 0.95 MHz
PEAK FREQUENCY -- 0.93 MHz
-6DB BANDWIDTH --- 58.25 %

COMMENTS:

F#: 0.85

** ACCEPTED

TECHNICIAN (3)

DATE: 07-08-2009

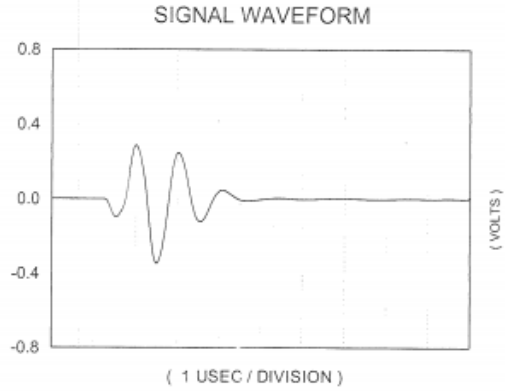

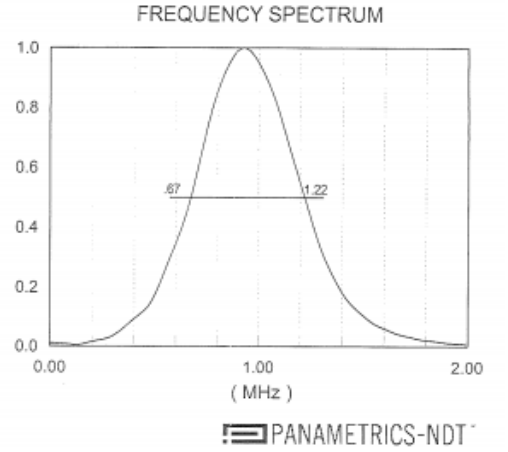

PANAMETRICS-NDT

For 2.25 MHz Shear Wave Contact Transducer

OLYMPUS

Tel: 781-419-3900
www.olympusndt.com

TRANSDUCER DESCRIPTION

PART NO.: V154
SERIAL NO.: 701051
DESIGNATION: CONTACT

FREQUENCY: 2.25 MHz
ELEMENT SIZE: .5 in. DIA.

TEST INSTRUMENTATION

PULSER/RECEIVER: PANAMETRICS 5052UA #1
DIGITAL OSCILLOSCOPE: LeCroy LT342 / SN: LT34202249
TEST PROGRAM: TP103-3 VER. 109CGN
CABLE: RG 174/U LENGTH: 4FT

TEST CONDITIONS

PULSER SETTING: ENERGY: 1 ; DAMPING: 50 OHM
RECEIVER SETTING: ATTN: 54dB ; GAIN: 40dB
TARGET: 1 IN SILICA
JOB CODE: TP200

MEASUREMENTS PER ASTM E1065

WAVEFORM DURATION:
-14DB LEVEL --- 0.560 US
-20DB LEVEL --- 0.640 US
-40DB LEVEL --- 1.320 US

SPECTRUM MEASURANDS:
CENTER FREQ. ------ 2.22 MHz
PEAK FREQUENCY -- 2.2 MHz
-6DB BANDWIDTH --- 95.7 %

COMMENTS:

WARNING! DO NOT EXCEED 150 VOLT EXCITATION PULSE.

Unit tested using uniform pressure system.
Sensitivity demonstrated on this certification
can only be duplicated under similar conditions.

** ACCEPTED

TECHNICIAN (3)

DATE: 04-06-2010

SIGNAL WAVEFORM

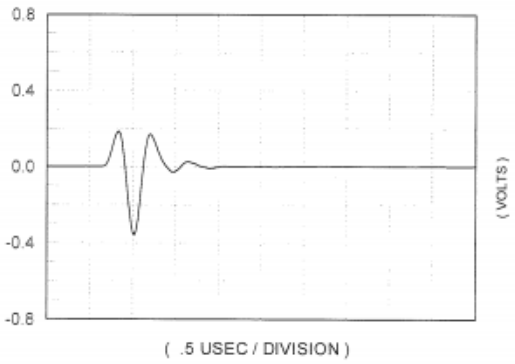

(.5 USEC / DIVISION)

FREQUENCY SPECTRUM

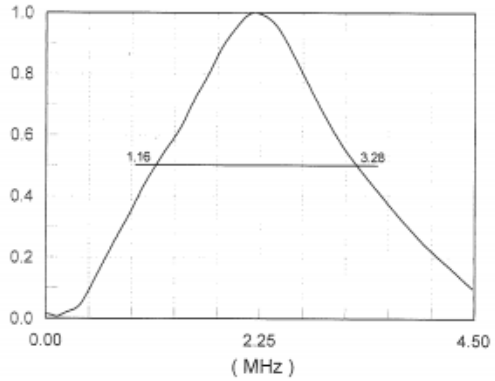

PANAMETRICS-NDT

Appendix C: Epoxy Material Safety and Datasheet

For Epothin Resin

MATERIAL SAFETY DATA SHEET

SECTION 1 – CHEMICAL PRODUCT AND COMPANY IDENTIFICATION

PRODUCT NAME: BUEHLER EPOTHIN RESIN
IDENTIFICATION NUMBER: 20-8140-032, 20-8140-128
PRODUCT USE/CLASS: Epoxy resin

SUPPLIER:
BUEHLER, a division of Illinois Tool Works Inc.
41 WAUKEGAN ROAD
LAKE BLUFF, IL 60044

EMERGENCY: 800-424-9300
INFORMATION: 847-295-6500
PREPARER: Technical Department, 847-295-6500
PREPARE DATE: 03/23/09, 23 March 2009

SECTION 2 – COMPOSITION/INFORMATION ON INGREDIENTS

ITEM	CHEMICAL NAME	CAS NUMBER	WT/WT%
01	Bisphenol-A Epoxy resin	25068-38-6	60.0-100.0
02	N-Butyl Glycidyl Ether	2426-08-6	10.0-30.0
03	Acrylic ester	TRADE SECRET	1.0-5.0
04	Diglycidyl ether	TRADE SECRET	1.0-5.0

ITEM	ACGIH TLV-TWA	ACGIH TLV-STEL	OSHA PEL-TWA	OSHA PEL – CEILING	COMPANY TLV-TWA	SKIN
01	N.E.	N.E.	N.E.	N.E.	N.E.	NO
02	25 ppm	N.E.	50 ppm	N.E.	5ppm-C NIOSH	NO
03	N.E.	N.E.	N.E.	N.E.	N.E.	NO
04	N.E.	N.E.	N.E.	N.E.	N.E.	NO

(SEE SECTION 16 FOR ABBREVIATION LEGEND)

SECTION 9 – PHYSICAL AND CHEMICAL PROPERTIES

BOILING RANGE:	327 - 500 F	VAPOR DENSITY:	Is heavier than air
ODOR:	Sweet	ODOR THRESHOLD:	No data
APPEARANCE:	Clear thin yellow	EVAPORATION RATE:	Is slower than Butyl Acetate
SOLUBILITY IN H_2O:	Negligible		
FREEZE POINT:	No data	SPECIFIC GRAVITY:	1.1299
VAPOR PRESSURE:	<0.1 mm@20 degC	pH @ 0.0%:	N.A.
PHYSICAL STATE:	Liquid	VISCOSITY:	Low
COEFFICIENT OF WATER/OIL DISTRIBUTION:		No data	

(SEE SECTION 16 FOR ABBREVIATION LEGEND)

For Epothin Hardener

MATERIAL SAFETY DATA SHEET

SECTION 1 – CHEMICAL PRODUCT AND COMPANY IDENTIFICATION

PRODUCT NAME: BUEHLER EPOTHIN HARDENER
IDENTIFICATION NUMBER: 20-8142-016, 20-8142-064
PRODUCT USE/CLASS: Epoxy hardener

SUPPLIER:
BUEHLER, a division of Illinois Tool Works Inc.
41 WAUKEGAN ROAD
LAKE BLUFF, IL 60044

EMERGENCY: 800-424-9300
INFORMATION: 847-295-6500
PREPARER: Technical Department, 847-295-6500
PREPARE DATE: 03/23/09, 23 March 2009

SECTION 2 – COMPOSITION/INFORMATION ON INGREDIENTS

ITEM	CHEMICAL NAME	CAS NUMBER	WT/WT%
01	Polyoxyalkylamine blend	NONE - MIX	30.0-60.0
02	Nonyl phenol	25154-52-3	5.0-10.0
03	Benzene-1,3-dimethaneamine	1477-55-0	10.0-30.0
04	Substituted phenol	TRADE SECRET	10.0-30.0
05	Triethylenetetramine	112-24-3	1.0-5.0
06	Trimethylhexanediamine	3236-53-1	10.0-30.0

ITEM	ACGIH TLV-TWA	ACGIH TLV-STEL	OSHA PEL-TWA	OSHA PEL – CEILING	COMPANY TLV-TWA	SKIN
01	N.E.	N.E.	N.E.	N.E.	N.E.	NO
02	N.E.	N.E.	N.E.	N.E.	N.E.	NO
03	N.E.	0.1 mg/m^3	N.E.	N.E.	0.1mg/m^3 (C)	NO
04	N.E.	N.E.	N.E.	N.E.	N.E.	NO
05	N.E.	N.E.	N.E.	N.E.	N.E.	NO
06	N.E.	N.E.	N.E.	N.E.	N.E.	NO

(SEE SECTION 16 FOR ABBREVIATION LEGEND)

SECTION 9 – PHYSICAL AND CHEMICAL PROPERTIES

BOILING RANGE:	278 - 500 F	VAPOR DENSITY:	Is heavier than air
ODOR:	Ammonia-like	ODOR THRESHOLD:	No data
APPEARANCE:	Clear thin	EVAPORATION RATE:	Is slower than Butyl Acetate
SOLUBILITY IN H_2O:	Appreciable		
FREEZE POINT:	No data	SPECIFIC GRAVITY:	0.97
VAPOR PRESSURE:	No data	pH @ 0.0%:	N.A.
PHYSICAL STATE:	Liquid	VISCOSITY:	Low
COEFFICIENT OF WATER/OIL DISTRIBUTION:		No data	

(SEE SECTION 16 FOR ABBREVIATION LEGEND)

Appendix D: Microballoon Properties

3M™ Glass Bubbles General Purpose Series

	Target Crush Strength (90% survival, psi)	True Density (g/cc)	Particle Size (microns, by volume) Distribution 10th%	50th%	90th%	Color (unaided eye)
K1	250	0.125	30	65	115	white
K15	300	0.15	30	60	105	white
S15	300	0.15	25	55	90	white
S22	400	0.22	20	35	65	white
K20	500	0.20	25	55	95	white
K25	750	0.25	25	55	90	white
S32	2000	0.32	20	40	70	white
S35	3000	0.35	10	40	75	white
K37	3000	0.37	20	45	80	white
XLD3000	3000	0.23	15	30	40	white
S38	4000	0.38	15	40	75	white
S38HS	5500	0.38	15	40	75	white
S38XHS	5500	0.38	15	40	70	white
K46	6000	0.46	15	40	70	white
XLD6000	6000	0.30	10	18	30	white
K42HS	8,000	0.42	11	22	37	white
S60	10,000	0.60	15	30	55	white
S60HS	18,000	0.60	11	30	50	white
IM30K	28,000	0.60	9	16	25	white

BIBLIOGRAPHY

ASTM D-695-85, "Standard Test Method for Compressive Properties of Rigid Plastics," pp. 199-204, 1988

ASTM E664 –93 (2005) Standard Practice for Measurement of the Apparent Attenuation of Longitudinal Ultrasonic Waves by Immersion Method, ASTM International, West Conshohocken, PA, USA

Bardella Lorenzo, Francesco Genna, On the elastic behavior of syntactic foams, International Journal of Solids and Structures, Volume 38, Issues 40-41, October 2001, Pages 7235-7260

Beltzer A. I. and N. Brauner,*Waves of an arbitrary frequency in random fibrous composites*. J. Acoust. Soc. Am.*76*, No. 3, 962-963 (1984) (also XVI. Int. IUTAM Congress, Lyngby, Denmark, August 1984).

Beltzer A.I. and N. Brauner, Acoustic waves in random discrete media via a differential scheme. *J. Appl. Phys.* **60** (1986), pp. 538–540.

Beltzer, Abraham I. Charles W. Bert, Alfred G. Striz, On wave propagation in random particulate composites, International Journal of Solids and Structures, Volume 19, Issue 9, 1983, Pages 785-791,

Beltzer, Abraham I. Neima Brauner, The dynamic response of random composites by a causal differential method, Mechanics of Materials, Volume 6, Issue 4, December 1987, Pages 337-345,

Biwa S., S. Idekoba, N. Ohno, Wave attenuation in particulate polymer composites: independent scattering/absorption analysis and comparison to measurements, Mechanics of Materials, Volume 34, Issue 10, October 2002, Pages 671-682

Biwa S., Independent scattering and wave attenuation in viscoelastic composites, Mechanics of Materials, Volume 33, Issue 11, November 2001, Pages 635-647

Biwa S., Y. Watanabe, N. Ohno, Analysis of wave attenuation in unidirectional viscoelastic composites by a differential scheme, Composites Science and Technology, Volume 63, Issue 2, February 2003, Pages 237-247

Biwa S., Y. Watanabe, S. Motogi, N. Ohno, Analysis of ultrasonic attenuation in particle-reinforced plastics by a differential scheme, Ultrasonics, Volume 43, Issue 1, October 2004, Pages 5-12

Brauner, N., A.I. Beltzer, Wave-obstacle interaction in a lossy medium: energy perturbations and negative extinction, Ultrasonics, Volume 26, Issue 6, November 1988, Pages 328-334,

Brauner, Neima, Abraham I. Beltzer, The Kramers-Kronig relations method and wave propagation in porous elastic media, International Journal of Engineering Science, Volume 23, Issue 11, 1985, Pages 1151-1162

d'Almeida J. R. M., An analysis of the effect of the diameters of glass microspheres on the mechanical behavior of glass-microsphere/epoxy-matrix composites, Composites Science and Technology, Volume 59, Issue 14, November 1999, Pages 2087-2091

Daniel I.M., S.C. Wooh, I. Komsky, J. Nondestruct. Eval. **11**, 1 (1992)

Datta S K.,A self-consistent approach to multiple scattering by elastic Ellipsoidal inclusions, J Appl Mech 1977 ; 44 : 657–62.

Drury J.C., NDT FUNDAMENTALS: ultrasonics, part 7. The ultrasonic beam, *Insight* **47** (5) (2005), pp. 297–299

Gubernatis, J. E., E. Domany, Effects of microstructure on the speed and attenuation of elastic waves in porous materials, Wave Motion, Volume 6, Issue 6, November 1984, Pages 579-589

Guoqiang Li, Nji Jones, Development of rubberized syntactic foam, Composites Part A: Applied Science and Manufacturing, Volume 38, Issue 6, June 2007, Pages 1483-1492

Gupta N., E. Woldesenbet, Patrick Mensah, Compression properties of syntactic foams: effect of cenosphere radius ratio and specimen aspect ratio, Composites Part A: Applied Science and Manufacturing, Volume 35, Issue 1, January 2004, Pages 103-111, ISSN 1359-835X

Gupta Nikhil, Eyassu Woldesenbet, Patrick Mensah, Compression properties of syntactic foams: effect of cenosphere radius ratio and specimen aspect ratio, Composites Part A: Applied Science and Manufacturing, Volume 35, Issue 1, January 2004, Pages 103-111

Gupta Nikhil, Raymond Ye, Maurizio Porfiri, Comparison of tensile and compressive characteristics of vinyl ester/glass microballoon syntactic foams, Composites Part B: Engineering, Volume 41, Issue 3, April 2010, Pages 236-245

Gupta Nikhil, William Ricci, Comparison of compressive properties of layered syntactic foams having gradient in microballoon volume fraction and wall thickness, Materials Science and Engineering: A, Volume 427, Issues 1-2, 15 July 2006, Pages 331-342

Hale J.M., J.N. Ashton, Ultrasonic attenuation in voided fibre-reinforced plastics, NDT International, Volume 21, Issue 5, October 1988, Pages 321-326

Hirone T. and T. Kamigaki, Attenuation of Ultrasonic Waves in Metals. I Aluminum, J. Japan Inst. Metals, 19 (1955),92

Hsiao H. M., I. M. Daniel, Strain rate behavior of composite materials, Composites Part B: Engineering, Volume 29, Issue 5, September 1998, Pages 521-533

Ishimaru, A.; "Theory and application of wave propagation and scattering in random media," *Proceedings of the IEEE* , vol.65, no.7, pp. 1030- 1061, July 1977

Jeong H. , Effects of Voids on the Mechanical Strength and Ultrasonic Attenuation of Laminated Composites *Journal of Composite Materials February 1997 31: 276-292*

Jhaver Rahul, Hareesh Tippur, Processing, compression response and finite element modeling of syntactic foam based interpenetrating phase composite (IPC), Materials Science and Engineering: A, Volume 499, Issues 1-2, Fifth International Conference on Physical and Numerical Simulations of Material Processing (ICPNS 2007) held at Zhengzhou, China, October 23-27, 2007, 15 January 2009, Pages 507-517

K. F. Graff, *Wave Motion in Elastic Solids* (Ohio State University Press, Columbus, 1975)

Kinra V K, Anand A.Wave propagation in a random particulate composite at Long and short wavelengths. Int J Solids Struct 1982;18(5):367–80.

Kolsky H 1963 Stress Waves in Solids. Dover, New York.

Layman Christopher, N. Sanjeeva Murthy, Ruey-Bin Yang, and Junru Wu, The interaction of ultrasound with particulate composites, J. Acoust. Soc. Am. 119, 1449 (2006)

M.W. Hyer, Stress analysis of fiber-reinforced materials, McGraw-Hill, New York (1997).

Martin, B.G., Ultrasonic attenuation due to voids in fibre-reinforced plastics, NDT International, Volume 9, Issue 5, October 1976, Pages 242-246

Mouritz, A. P., Ultrasonic and Interlaminar Properties of Highly Porous Composites, Journal of Composite Materials 2000 34: 218-239

Mouritz, A.P., Ultrasonic & interlaminar properties of highly porous composites, *J Compos Mater* **34** (2000) (3), pp. 218–239.

Mylavarapu Phani, Woldesenbet, Eyassu, 'Ultrasonic Characterization of Sandwich Core Materials', Journal of Sandwich Structures and Materials 2008 10: 413-428

Mylavarapu Phani, Woldesenbet, Eyassu, A predictive model for ultrasonic attenuation coefficient in particulate composites, Composites Part B: Engineering, Volume 41, Issue 1, January 2010, Pages 42-47, ISSN 1359-8368
Nair S.M., D.K. Hsu, J.H. Rose, J. Nondestruct. Eval. **8**, 13 (1989)

Rajendran V., N. Palanivelu, B.K. Chaudhuri, A device for the measurement of ultrasonic velocity and attenuation in solid materials under different thermal conditions, Measurement, Volume 38, Issue 3, October 2005, Pages 248-256

Rohatgi, P. K., Matsunaga, T. and Gupta, N., Compressive and ultrasonic properties of polyester/fly ash composites. Journal of Materials Science, 2009. 44(6): p. 1485-1493.

Song B., W. Chen and D.J. Frew, *J. Compos. Mater.* **38** (2004), pp. 915–936

Song Bo, Weinong Chen, Tamaki Yanagita, Danny J. Frew, Temperature effects on dynamic compressive behavior of an epoxy syntactic foam, Composite Structures, Volume 67, Issue 3, Dynamic Response of Advanced Materials and Structures, March 2005, Pages 289-298

Song, Bo, Chen, Weinong, Frew, Danny J., Dynamic Compressive Response and Failure Behavior of an Epoxy Syntactic Foam, Journal of Composite Materials 2004 38: 915-936

Truel R., C. Elbaum, and B. Chick, *Ultrasonic Method in Solid State Physics* (Academic, New York, 1969).

Woldesenbet E. and S. Peter, Volume fraction effect on high strain rate properties of syntactic foam composites, *J Mater Sci* **40** (15) (2009), pp. 4009–4017.

Woldesenbet E., N. Gupta and H. Jerro, Effect of microballoon radius ratio on syntactic foam core sandwich composites, *J Sandwich Struct Mater* **7** (2) (2005), pp. 95–111

Woldesenbet Eyassu, Low velocity impact properties of nanoparticulate syntactic foams, Materials Science and Engineering: A, Volume 496, Issues 1-2, 25 November 2008, Pages 217-222

www.3m.com, 3M™ Microspheres Selection Guide. (2009). Retrieved April 11, 2009, from, http://multimedia.3m.com/mws/mediawebserver?mwsId=66666UuZjcFSLXTtlXM6LxfXEVuQEcuZgVs6EVs6E666666--&fn=MicroSelectGuide_DMR.pdf

www.ndt-ed.org, Reflection and Transmission Coefficients (Pressure), (2001). Retrieved March 4, 2009, from http://www.ndt-ed.org/EducationResources/CommunityCollege/Ultrasonics/Physics/reflectiontransmission.htm

www.olympus-ims.com, Olympus Transducer Catalog, (2009), Retrieved August 11, 2009, from http://www.olympus-ims.com/data/File/panametrics/panametrics-UT.en.pdf

Ying C F, Truell R. 'Scattering of a plane longitudinal wave by a spherical Obstacle in an isotropically elastic solid'. J Appl Phys 1956; 27(9):1086–97.